AGU100 ADVANCING EARTH AND SPACE SCIENCE

Tectonics

RESEARCH ARTICLE
10.1029/2018TC005152

Special Section:
Geodynamics, Crustal and Lithospheric Tectonics, and active deformation in the Mediterranean Regions (A tribute to Prof. Renato Funiciello)

Palinspastic Reconstruction Versus Cross-Section Balancing: How Complete Is the Central Taurides Fold-Thrust Belt (Turkey)?

Peter J. McPhee[1], Douwe J. J. van Hinsbergen[1], Marco Maffione[2], and Demir Altıner[3]

[1]Department of Earth Sciences, Utrecht University, Utrecht, Netherlands, [2]Department of Earth Sciences, University of Birmingham, Edgbaston, Birmingham, UK, [3]Department of Geological Engineering, Middle East Technical University, METU Üniversiteler Mah, Ankara, Turkey

Key Point:
- Wholesale underthrusting was the dominant process in Taurides accretion and led to a highly incomplete shortening record of convergence

Supporting Information:
- Supporting Information S1
- Data Set S1

Correspondence to:
P. J. McPhee,
p.j.mcphee@uu.nl;
peter.mcphee@live.co.uk

Citation:
McPhee, P. J., van Hinsbergen, D. J. J., Maffione, M., & Altıner, D. (2018). Palinspastic reconstruction versus cross-section balancing: How complete is the central Taurides fold-thrust belt (Turkey)? *Tectonics*, *37*. https://doi.org/10.1029/2018TC005152

Received 22 MAY 2018
Accepted 6 OCT 2018
Accepted article online 12 OCT 2018

Abstract In many fold-thrust belts, cross section–derived shortening estimates are significantly lower than predicted based on plate convergence. This has led to controversial hypotheses that shortening may be largely underestimated due to wholesale underthrusting (convergence without shortening) below far-traveled continent or ocean-derived nappes. The Late Cretaceous-Eocene Taurides fold-thrust belt (southern Turkey) may contain a highly incomplete shortening record of convergence likely caused by wholesale underthrusting. To estimate this underthrusting, we calculate convergence across the belt using a map-view palinspastic reconstruction that takes into account major rotations of tectonic units during their accretion. We use paleomagnetic and fault kinematic analysis, timing of accretion, and Africa-Eurasia convergence to constrain our reconstruction. Our paleomagnetic results confirm an ~40° clockwise vertical axis rotation of the Geyikdağı nappe that forms the core of the belt, which we interpret is accommodated by a lateral gradient in underthrusting on faults structurally above and below the Geyikdağı nappe. We reconstruct ~400–450 km of convergence across the Taurides during their accretion. We compare this predicted convergence to shortening calculated from balanced cross sections, in which we reconstruct a minimum of 154-km shortening: 57 km within far-traveled nappes, 70-km thrusting of far-traveled nappes over the Geyikdağı nappe, and 27-km shortening within the Geyikdağı nappe. Shortening in the Taurides created a significant nappe stack, but the majority of convergence was accommodated by wholesale underthrusting with barely a trace at the surface, including ~160 km of convergence by rotation of the belt, and 90–130 km related to missing Africa-Eurasia convergence.

1. Introduction

Estimates of crustal shortening derived from balanced cross sections are widely used in paleogeographic reconstructions to assess the geodynamic and plate kinematic context of orogenesis (e.g., McQuarrie, 2002; Muñoz, 1992; Woodward et al., 1989). Restoring shortening is for instance useful to assess the role of continental subduction in fold-thrust belt evolution (Beaumont et al., 2000; van Hinsbergen et al., 2005; Long et al., 2011; Tate et al., 2015). In absence of constraint, balanced cross sections are reconstructed with an assumption of minimum shortening (i.e., the distance over which a body of rock decreased in horizontal width, accommodated by folding and thrusting), meaning that a final shortening estimate derived from a cross section is a minimum estimate of convergence (i.e., the distance over which two points move toward each other) taken up across the orogen. Even if all convergence is accommodated and recorded by shortening, the erosion of hanging wall anticlines associated with thrust faults may lead to an underestimate of shortening in a reconstruction. However, if the décollement horizon coincides with the top of the stratigraphy in a downgoing plate, there is no accretion of rock, and thus no shortening record—a mode that we here refer to as *wholesale subduction*, or *wholesale underthrusting*. In such settings, the amount of convergence accommodated may be orders of magnitude higher than the amount of shortening.

In studies focused on, for example, resource exploration, an assumption of minimum shortening may be used to build predictive structural models of the subsurface (e.g., Roeder, 2010). Paleogeographic and plate tectonic reconstructions, however, aim to portray the entire paleo-Earth surface, and so in these reconstructions, restoring wholesale underthrusting is essential.

Oceanic subduction zones often accommodate wholesale underthrusting—it is, in fact, the default mode. Large amounts of convergence (e.g., resulting in closure of entire ocean basins) may be accommodated without a volumetrically significant record of shortening by accretion or by shortening in the overriding plate. For instance, the Indus-Yarlung suture zone in the Himalaya, the Main Zagros Thrust in the Zagros mountain belt, or the Izmir-Ankara suture zone (IASZ) in Turkey are thought to have accommodated thousands of km of subduction leaving only narrow zones of mélange in the geological record (Gansser, 1980; Sengör & Yilmaz, 1981; Takin, 1972). Fold-thrust belts also commonly contain far-traveled continent-derived nappes or oceanic nappes in the form of ophiolites, on which wholesale underthrusting is difficult to quantify (e.g., McQuarrie & van Hinsbergen, 2013). The most straightforward way to quantify wholesale underthrusting is to compare estimates of shortening with either independently calculated syn-orogenic plate convergence based on global marine magnetic anomaly-based plate reconstructions (e.g., Nicol & Beavan, 2003), or paleomagnetic data (e.g., Huang et al., 2015). In many fold-thrust belts, cross section–derived shortening estimates are significantly lower than predictioned plate convergence. This has led to controversial hypotheses that shortening in orogenic belts that are dominated by far-traveled nappes may be largely underestimated. Such debates are ongoing in for example the Caucasus (Cowgill et al., 2016, 2018; Vincent et al., 2018), the Pyrenees (Barnett-Moore et al., 2016, 2017; van Hinsbergen, Spakman, et al., 2017; Vissers et al., 2016), and the Himalayas (Aitchison & Ali, 2012; DeCelles et al., 2014; van Hinsbergen et al., 2012a, 2012b, 2018; van Hinsbergen, Lippert, et al., 2017; Ingalls et al., 2016; Rowley & Ingalls, 2017). In these examples it has been suggested that thrust faults between continental-derived nappes may either represent cryptic suture zones that once accommodated oceanic subduction or major wholesale continental subduction. Without an exposed geological record, the role of wholesale lithosphere subduction—oceanic or continental—remains notoriously difficult to unequivocally demonstrate. On the other hand, as exemplified by the limited accretionary record despite thousands of km of Cenozoic subduction below the Andes (e.g., Oncken et al., 2006; Schepers et al., 2017), absence of evidence may not be evidence of absence.

In this paper, we aim to assess the role of wholesale underthrusting during the Late Cretaceous to Eocene age formation of the Taurides fold-thrust belt in southern Turkey (Figure 1). The Taurides consist of far-traveled nappes that were thrust over the internally thrusted Geyikdağı nappe in Eocene times (McPhee et al., 2018; Özgül, 1984). A recent balanced cross section across the Taurides by McPhee et al. (2018) documented a minimum of 55 km of shortening accommodated by thrusting of the far-traveled nappes over the Geyikdağı nappe. In addition, a minimum of 18 km of shortening was associated with duplexing within the underlying Geyikdağı nappe, suggesting that at least 73 km of convergence was accommodated across the belt in Eocene times. There is evidence to suggest that this estimate of minimum convergence is quite incomplete and that much more convergence may have been accommodated across the belt. First, despite continuous Africa-Europe convergence, the Taurides appear to have accreted in two short intervals, separated by a long period without accretion, in Late Cretaceous and then Eocene times. Second, existing paleomagnetic data suggest that the Geyikdağı nappe was affected by a ~40° clockwise (CW) vertical axis rotation, during or shortly after its accretion in Eocene time (Cinku et al., 2016; Kissel et al., 1993; Meijers et al., 2011). The rotation of the Taurides was therefore most likely accommodated on thrust faults associated with the fold-thrust belt. The CW rotation may have affected a domain up to ~200 km long, based on structural trends, requiring a lateral gradient in shortening on the order of tens to more than a hundred kilometers.

The combined constraints on Africa-Europe convergence, timing of accretion of major nappes from the downgoing to the upper plate, and paleomagnetic constraints on vertical axis rotations allow us to develop a map view (i.e., palinspastic) restorations of tectonic and paleogeographic evolution (e.g., van Hinsbergen & Schmid, 2012) independently of balanced cross-section constraints. We may therefore assess the magnitude of wholesale continental underthrusting for which there is virtually no accretionary record.

For our analysis, we used three independent techniques. First, we collected new paleomagnetic data from seven new sites in the Geyikdağı nappe to test the robustness and regional extent of the previously calculated rotations and to determine the occurrence and entity of local rotations within the Geyikdağı nappe. Second, we collected fault kinematic data on major faults to test whether thrusting was oblique or dip slip compared to the mapped structural trends in the belt. Third, we built a new first-order balanced cross section through the Eocene belt, ~80 km to the southeast of the cross section reconstructed by McPhee et al. (2018) to test for along-strike variations in both structural style and shortening. Finally, we combined our and

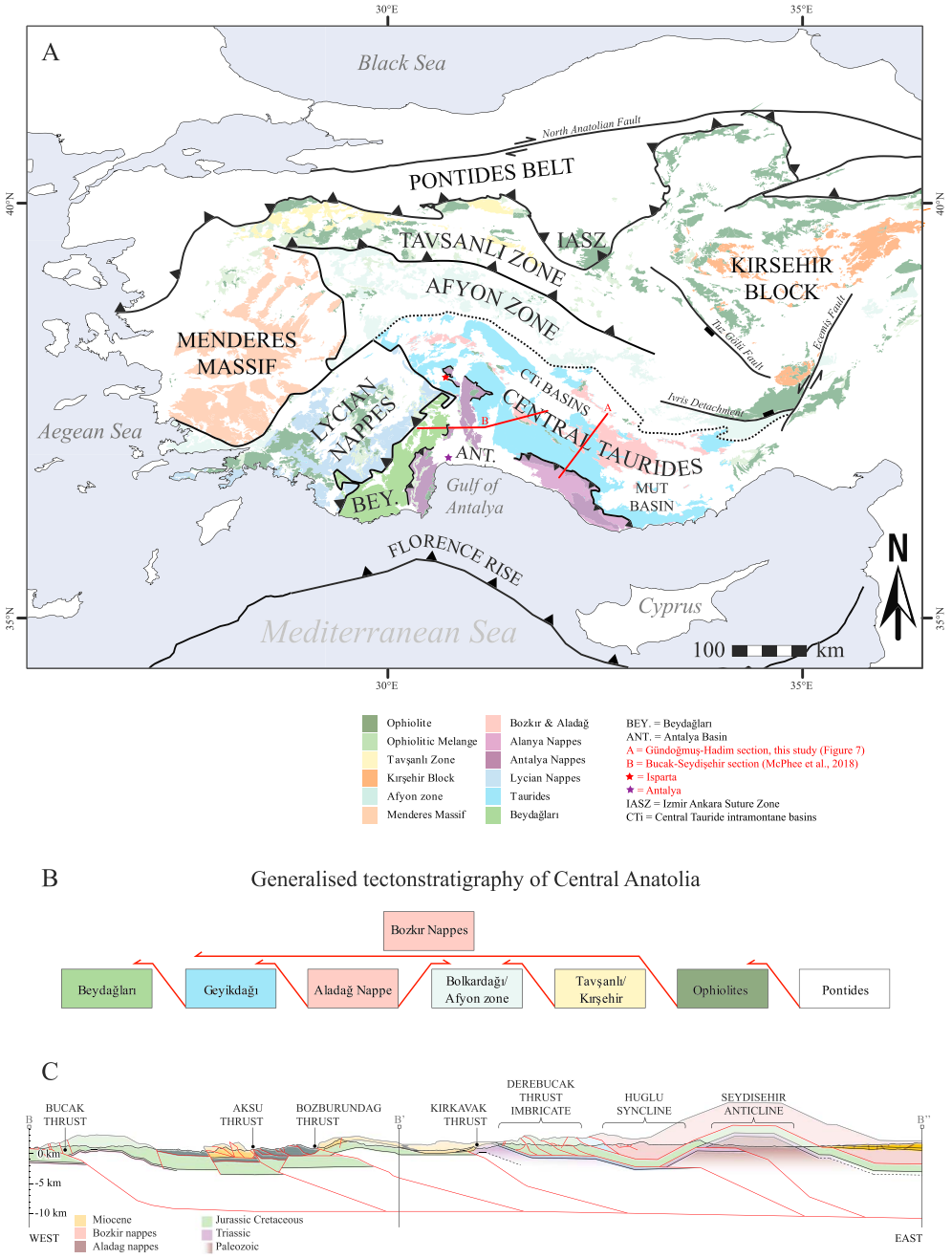

Figure 1. (a) Map of and tectonic units of western and central Turkey based on the MTA 1:500,000 geological map series. The locations of the Bucak-Seydişehir section (McPhee et al., 2018) and our new Gündoğmuş-Hadim section are indicated as red lines. (b) Tectonostratigraphy of the major units of western and central Turkey based on van Hinsbergen et al. (2016) and references therein. (c) Bucak-Seydişehir section of McPhee et al. (2018), showing generalized stratigraphy, and major structural elements of the belt, which we refer to in later sections.

previously published paleomagnetic data within a map view palinspastic reconstruction of the Central Taurides, from 100 Ma to Present.

2. Geological Setting

Anatolia (modern Turkey) contains a Late Cretaceous to middle Eocene orogen composed of continent-derived upper crustal nappes, which are locally covered by ophiolites. Accretion of these nappes is

thought to be the result of continental and oceanic subduction below an oceanic upper plate lithosphere (Gürer et al., 2016; Menant et al., 2016; Sengör & Yilmaz, 1981; van Hinsbergen et al., 2016). These nappes consist of a high-grade metamorphic domain in northern and central Anatolia (e.g., Okay, 1986) and a nonmetamorphic fold-thrust belt in the south known as the Taurides (e.g., Özgül, 1976; Figure 1). This wide orogenic system formed by deformation of the eastern part of a microcontinent known as Greater Adria (Gaina et al., 2013) or the Adria-Turkey plate (Stampfli et al., 1991), which was separated from Eurasia in the north and from Africa in the south by the Neotethys Ocean.

Closure of the Neotethys Ocean led to the formation of the E-W trending IASZ (Figure 1) and was accommodated by two subduction zones that formed in the Early Jurassic and Late Cretaceous (e.g., Barrier & Vrielynck, 2008; Gürer et al., 2016; van Hinsbergen et al., 2016; Moix et al., 2008; Okay, 1986; Pourteau et al., 2010; Robertson, 2004; Robertson et al., 2009; Sengör & Yilmaz, 1981). The northern subduction zone was located along the southern margin of Eurasia since at least the Early-Middle Jurassic and consumed oceanic Neotethyan lithosphere (Maffione & van Hinsbergen, 2018; Topuz et al., 2013). The southern subduction zone started in the Late Cretaceous along intraoceanic fracture zones and the passive margin of Greater Adria (e.g., Aldanmaz et al., 2009; Çelik et al., 2006; Dilek et al., 2007; Gürer et al., 2016; Maffione et al., 2017; Okay, 1986; Parlak et al., 2013; Sengör & Yilmaz, 1981; van Hinsbergen et al., 2016). After IASZ formed by closure of the Neotethys north of Greater Adria, the southern subduction zone remained active and accommodated the underthrusting of Greater Adria continental lithosphere, resulting in accretion of the nappes that make up the Anatolian orogen. The IASZ is a simple E-W trending suture and formed by ~N-S Africa-Eurasia convergence (Gaina et al., 2013; e.g., Seton et al., 2012). Despite this first-order simplicity, the modern distribution of tectonic units and metamorphic belts that formed by progressive accretion to the south of the IASZ varies strongly along-strike (see van Hinsbergen et al., 2016 for a comprehensive review; Figure 1). This may be a result of the original shape of the Greater Adriatic margin, and the shape of the Cretaceous subduction zone that was made up of ~N-S and ~E-W segments roughly following the Adriatic passive margin (van Hinsbergen et al., 2016; Lefebvre et al., 2013; Maffione et al., 2017; Gürer & van Hinsbergen, 2018). According to these reconstructions, the area in Central Anatolia investigated in this study formed adjacent to an ~N-S trending subduction zone.

Three belts of high grade metamorphic rocks are exposed to the north and east of, and structurally above the Taurides (Figure 1). These represent the deeply underthrusted, metamorphosed, and exhumed remnants of the northern Greater Adria microcontinent. The northernmost of these are the Tavşanlı zone and the Kırşehir block in western and central Turkey, respectively (Okay, 1986; Plunder et al., 2015; Pourteau et al., 2018; Sengör & Yilmaz, 1981; Whitney et al., 2003; Whitney et al., 2014), which form the structurally highest units below the Upper Cretaceous ophiolites and are probably lateral paleogeographic equivalents. They contain coeval ages of peak metamorphism at ~85 Ma, but the metamorphic rocks in those zones experienced different pressure and temperature conditions (van Hinsbergen et al., 2016, and references therein; Pourteau et al., 2018). The Afyon zone is located to the south of the Kırşehir block and Tavşanlı zone. It is structurally below the Tavşanlı zone and is likely to be structurally below the Kırşehir block, but no contact is exposed. The Afyon zone consists of continent derived HP/LT rocks that experienced peak metamorphism at ~65 Ma (Candan et al., 2005; Okay, 1984; Özdamar et al., 2013; Pourteau et al., 2010, 2013). Metamorphic rocks in the Afyon zone are locally covered by Paleocene-Eocene marine sedimentary rocks (Candan et al., 2005; Gürer et al., 2016), which demonstrate rapid exhumation of the metamorphic units. Exhumation was accommodated along extensional detachments in a long-lived, Late Cretaceous to early Eocene back-arc basin (Gürer, Plunder, et al., 2018) that, when corrected for Eocene and younger vertical axis rotations (Lefebvre et al., 2013; Gürer, van Hinsbergen, et al., 2018), accommodated E-W extension.

To the south of the metamorphic units, the Tauride fold-thrust belt consists of nonmetamorphic nappes and forms the southern margin of the Central Anatolian Plateau (Figure 1). The Central Taurides are represented by a Late Cretaceous to Eocene thin-skinned fold-thrust belt that broadly consists of three major tectonostratigraphic units. In this contribution we will follow the tectonostratigraphic nomenclature of Özgül (1984) and McPhee et al. (2018). The Bozkır nappes are the highest tectonostratigraphic unit in the Central Taurides and contain dismembered ophiolite rocks and ophiolitic mélange composed of deformed Triassic to Upper Cretaceous volcanic and sedimentary rocks (Andrew & Robertson, 2002; Çelik & Delaloye, 2006; Gutnic et al., 1979; Özgül, 1984).

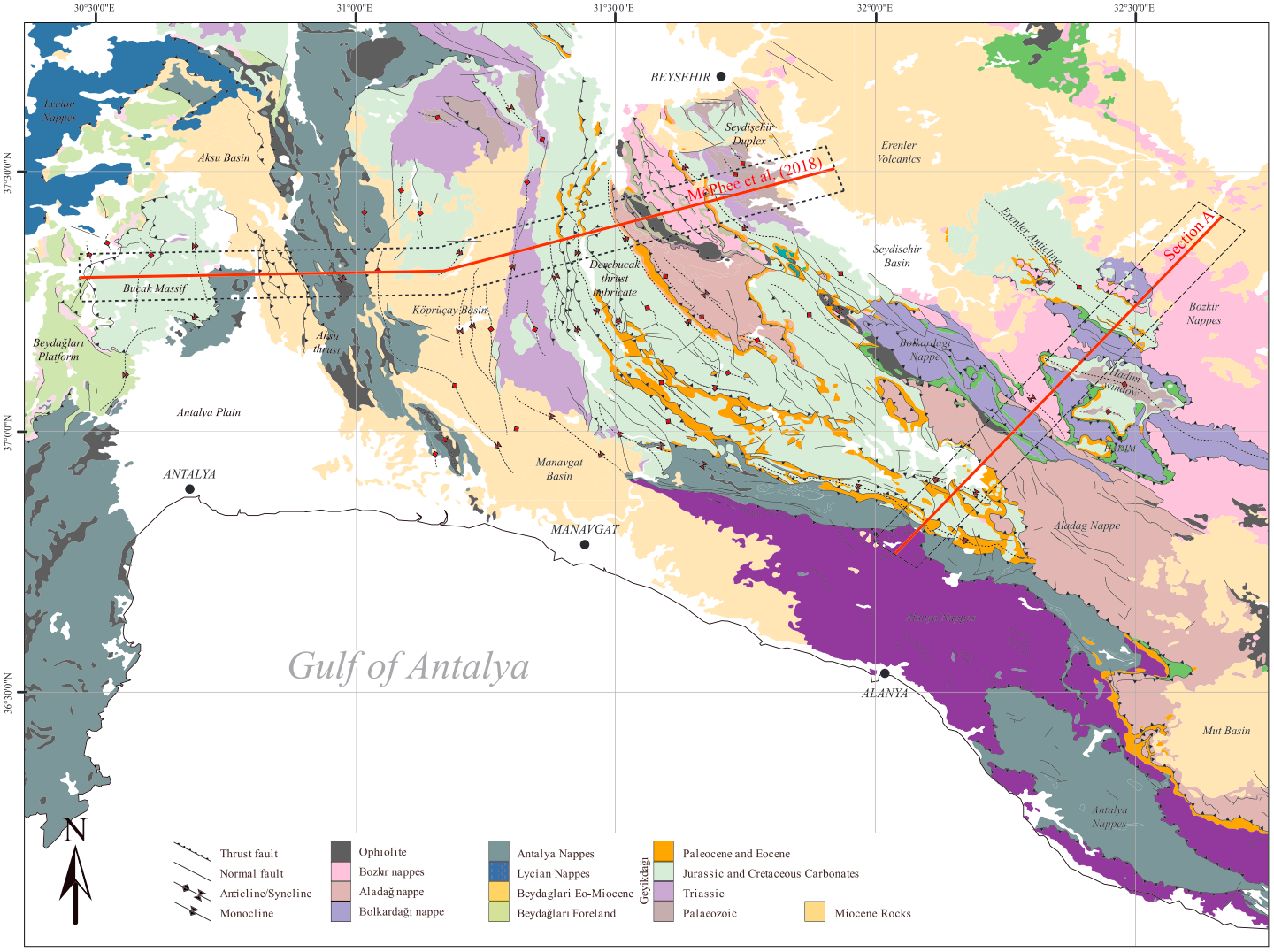

Figure 2. Small-scale map showing generalized geological units and major faults and folds in the western central Taurides based on the MTA 1:500,000 geological map series. The extent of our strip map (Figure 6) is shown by the red dashed box.

The next major units consist of coherent nappes of Paleozoic to Upper Cretaceous platform carbonates known as the Bolkardağı nappe and the Aladağ nappe. These nappes were likely part of a continuous platform since Late Permian times with differences in Carboniferous to Permian stratigraphic thickness caused by basin geometry (Altiner et al., 2000; Özgül, 1976, 1984). The Aladağ nappe is rootless and is situated to the south of the Bolkardağı nappe. The Bolkardağı nappe is nonmetamorphic at its contact with the Aladağ nappe in the south and is affected by an increasingly high grade of metamorphism towards the north where it is known as the Afyon zone (Demirtasli et al., 1984). The Aladağ nappe is covered by a sedimentary mélange that contains sedimentary rocks no younger than Maastrichtian age, which constrain its accretion at ~66 Ma (Mackintosh & Robertson, 2013).

The Bozkır nappes and the Aladağ and Bolkardağı nappes are thrust for at least 50 km over the now internally imbricated Geyikdağı nappe, based on the distribution of tectonic windows and klippen (Figure 2). The Geyikdağı nappe broadly consists of an upward shallowing sequence of Triassic to middle Eocene carbonate rocks, deposited on Ordovician and older continental basement (Gutnic et al., 1979; Monod, 1977; Özgül, 1976, 1984). The Geyikdağı nappe was deformed by a thin-skinned thrust fault imbricate system that affected the uppermost Mesozoic carbonates and by a deeper thrust duplex system that incorporates Ordovician and older basement rocks (McPhee et al., 2018). The Bozkır, Aladağ, and Bolkardağı nappes, which are

allochthonous, were thrust onto the Geyikdağı nappe in late Lutetian time (middle Eocene, ~41 Ma), as constrained by the youngest synorogenic (*flysch*) rocks in the underthrusted Geyikdağı stratigraphy (Gutnic et al., 1979; Monod, 1977).

There is scarce geological evidence for the tectonic history of the Central Taurides between the Late Cretaceous accretion of the Aladağ and Bolkardağı nappes, and the middle Eocene accretion and thrusting of the Geyikdağı nappe. While there is stratigraphic evidence to suggest that the Jurassic and Cretaceous platform rocks of the Geyikdağı nappe may grade into the Aladağ and Bolkardağı nappes (Altiner et al., 2000), there are thin slivers of deeper marine sedimentary rocks up to Campanian-Maastrichtian that are found at the Aladağ-Geyikdağı thrust contact (Mackintosh & Robertson, 2013; Özgül, 1984). Those rocks may represent an basin that once separated the Aladağ and Geyikdağı platforms.

After the middle Eocene, Africa-Europe convergence was accommodated by oceanic subduction to the south of the Taurides, meaning that the Beydağları platform and overlying Tauride fold-thrust belt were located in an upper plate position (McPhee et al., 2018; van Hinsbergen et al., 2010). A slab remnant containing the original lower crustal and mantle lithospheric underpinnings of the Central Taurides may still be found below southern Turkey and Cyprus (van Hinsbergen et al., 2010; Koç, van Hinsbergen, et al., 2016; Koç, Kaymakci, et al., 2016; McPhee et al., 2018) and probably is represented by the Antalya slab (Biryol et al., 2011; van der Meer et al., 2018), which was likely decoupled from the African plate in late Eocene time.

Following an apparent period of tectonic quiescence in the northwestern Central Taurides, the Eocene fold-thrust belt was partly refolded and thrusted by a western belt of thrusting that deformed the Geyikdağı and Beydağları platforms and the overlying Miocene to Pliocene Antalya basin. Miocene and younger thrusting in the belt was coeval with the formation of a regional system of extensional basins in the Tauride hinterland to the northeast of the range (Koç et al., 2012, 2017, 2018) and was associated with oroclinal bending of the Central Taurides (Koç, van Hinsbergen, et al., 2016; Figure 1). Koç, van Hinsbergen, et al. (2016) found that the orocline formed by a 20°–30° CW rotation of the Köprüçay subbasin in the north, and a 25°–35° anticlockwise (ACW) rotation of the Manavgat subbasin to the south, which must have been accommodated by motion on the Miocene Bozburundağ and Aksu thrusts that are structurally below the orocline because the Aksu basin to the west did not rotate (Figure 2). In the east, the Miocene oroclinal rotations must have been accommodated by extension within the Central Tauride basin province in the Tauride hinterland (Figure 1). The Miocene oroclinal bending therefore affected the Eocene rocks of the Taurides. Koç et al. (2018) recently made a kinematic restoration of the Miocene extension, shortening, and oroclinal bending, and we use their results as basis for our restoration of the pre-Neogene deformation history of the Tauride belt.

The Central Taurides also contain a Late Cretaceous-Paleocene nappe stack known as the Antalya-Alanya nappes, which were emplaced northward onto the southern margin of the Geyikdağı and Beydağları platforms. North-verging thrust faults in the Antalya-Alanya nappes are unconformably overlain by Paleocene nummulitic limestone (Özgül, 1984), indicating that northward thrusting ended long before south verging and propagating deformation arrived in the Taurides. The emplacement of the nappe stack is interpreted as the result of westward roll-back and invasion of a subduction zone to the south of the Taurides (Maffione et al., 2017; Moix et al., 2008). The emplacement and shortening of the Antalya-Alanya nappes thus did not accommodate Africa-Europe convergence and is unrelated to the shortening versus convergence problem we address in this paper.

The Geyikdağı nappe was affected by a post-Late Cretaceous remagnetization event of presumed Eocene age: the precise extent of remagnetization is uncertain (Meijers et al., 2011). Paleomagnetic data from Eocene units of the Geyikdağı nappe indicate a post-middle Eocene ~40° CW rotation (Cinku et al., 2016; Kissel et al., 1993; Meijers et al., 2011;). Vertical axis rotations are an expression of lateral strain variations. Elsewhere in the Mediterranean, major rotations in fore-arc settings, as seen in the Taurides, are often accommodated by differential back-arc extension (e.g., Cifelli et al., 2007; van Hinsbergen & Schmid, 2012). Back-arc extension has been reported in Turkey, but it predates the middle Eocene (e.g., Seyitoglu et al., 2017; Gürer, Plunder, et al., 2018) and therefore predates rotation of the Taurides. The rotation of the belt is therefore most likely accommodated by thrust faults. The lateral extent of the rotated domain is poorly constrained. There is no depositional record in the Western Taurides for the late middle Eocene-early Miocene interval, and the

Antalya basin was not affected by an ~40° CW rotation (Kissel et al., 1993). This constrains the regional rotation of the Geyikdağı nappe to the time interval between ~40 and 20 Ma.

3. Methods

3.1. Paleomagnetic Data

Oriented paleomagnetic cores were collected from seven sites across the western Central Taurides to test robustness of the previously reported CW rotation of the Geyikdağı nappe and to evaluate whether differential rotations occurred between different thrust sheets. We sampled Eocene marine siltstone (2 sites), nummulitic limestone (3 sites), and fine-grained marine sandstone (2 sites) from the uppermost sedimentary units of the Geyikdağı stratigraphy. Paleomagnetic cores (25-mm diameter) were drilled with a petrol-powered, water-cooled portable drill, and then cut in the lab into standard 22-mm-long specimens. Cores and bedding plane orientations were measured in the field using a magnetic compass corrected for the local declination of 5°E. At each site, 5 to 14 samples were collected over an ~20-m stratigraphic thickness to ensure that paleosecular variation (PSV) of the geomagnetic field was adequately sampled.

Specimens were subjected to stepwise thermal demagnetization in a shielded oven (ASC TD48-SC) at the paleomagnetic laboratory "Fort Hoofddijk" (Utrecht University). Temperature increments of 20–50 °C were applied from room temperature up to a maximum of 580 °C. The magnetic remanence was measured after each demagnetization step on a horizontal 2G DC SQUID cryogenic magnetometer (noise level 3×10^{-12} Am^2). Demagnetization data were plotted on orthogonal diagrams (Zijderveld, 1967), and principal component analysis (Kirschvink, 1980) and statistical analysis were carried out using online software paleomagnetism.org (Koymans et al., 2016). The original Zijderveld diagrams, their interpretations, and statistical analysis from this study are provided in Supplementary file DS01 and can be imported into paleomagnetism.org software. Characteristic remanent magnetization (ChRM) directions were calculated mainly using best fit lines, but great circles (McFadden & McElhinny, 1988) were also used in samples showing partial demagnetization. Site mean directions and associated declination (ΔD_x) and inclination (ΔI_x) errors were determined using Fisher statistics (Fisher, 1953) applied on virtual geomagnetic poles (VGPs) corresponding to the isolated ChRMs (Deenen et al., 2011). A fixed 45° cutoff to the VGP/ChRM distributions was applied before computing the mean values (Deenen et al., 2011; Johnson et al., 2008). Fold tests (Tauxe, 2010; Tauxe & Watson, 1994) could not be performed due to the low variability of the bedding plane orientation across the sampled sites. Quality criteria of Deenen et al. (2011) using VGP distribution at the site level were instead adopted to assess the preservation of the primary remanence in the studied rocks. Underrepresentation of PSV reflected in a tighter VGP clustering than expected (i.e., $A_{95} < A_{95min}$) may indicate either remagnetization or a nonaveraged record of the geomagnetic field (hence not reliable for tectonic interpretations). On the other hand, overrepresentation of PSV identified by a larger VGP scattering than predicted (i.e., $A_{95} > A_{95max}$) may denote the occurrence of pervasive deformation at the site level or an inefficient preservation of the remanence.

3.2. Fault Kinematics

The modern structural trend of the belt is oblique to Africa-Eurasia convergence, and so we aimed to see if this led to oblique thrusting. Fault slip data were collected at major thrust zones within the Central Taurides (results shown in Figure 5a) to investigate whether faulting within the CW rotated domain was overall dip slip or oblique. We also collected fault slip data along high angle faults that cut through the cross section.

We identified major thrusts by stratigraphic separation across faults mapped in the MTA 1:500,000 scale geological map of the region and by following the structural interpretation of McPhee et al. (2018). At each location we measured as many individual fault planes with preserved kinematic indicators within the fault zone as possible. Where possible, offset marker beds were used as sense of slip indicators, but we largely relied on slickensides as sense of slip indicators, and those included striations, trailed material, mineral fibers, and steps in the fault plane. We found no exposure of well-preserved slickensides in two important thrust zones, and so we inferred the transport direction on those faults by measuring folding in footwall sedimentary rocks. We did not correct fault orientation for bedding dip because the

thrusts we measured deform shallow to moderately dipping beds. Fault kinematic data are presented as Angelier plots (Figure 5).

3.3. Cross Section Construction

In this study, we developed a first-order balanced and restored cross section of the Central Tauride fold-thrust belt. We compared this to a previous section: the Bucak-Seydişehir built by McPhee et al. (2018; section Figure 1c), to test for an along-strike variation in structural style and magnitude of shortening in the Geyikdağı nappe. Since shortening contained in the Antalya-Alanya nappes predated the Eocene (south verging and propagating) fold thrust-belt that we are interested in and did not accommodate Africa-Europe convergence but subduction roll-back, which was balanced by upper plate extension (Maffione et al., 2017), we treated those nappes as a single undifferentiated passive unit and did not include internal shortening there in our shortening estimate. To this end, we first surveyed a strip map across the belt, which was orthogonal to the average bedding strike, and so approximately parallel to the transport direction of the thrust faults (as constrained by our fault kinematic data; Gündoğmuş-Hadim section, Figure 2). We mapped lithostratigraphy, and major folds and faults within the strip map area, and also made field observations in the surrounding region to inform our interpretations. We interpreted thrust faults where we saw lithostratigraphic repetitions or evidence for footwall cutoff and hanging wall cutoff relationships. We projected nearby dip measurements and boundaries onto the chosen cross section using Move 2016.1 and constructed our section using dip panels (i.e., domains of similar dip, separated by bisecting axial planes) in Adobe Illustrator.

The geometry of a thrust fault has a first-order control on hanging wall deformation (e.g., Berger & Johnson, 1980; Woodward et al., 1989). We therefore used exposed hanging wall deformation to predict subsurface fault geometry. We assumed that steep bedding are caused by an underlying thrust fault ramp, or a stack of ramps, and so we used changes from shallow to steep bedding to predict the position of underlying thrust fault ramps (e.g., Suppe, 1983). At each step in building the cross section, we assumed the simplest structural solution with the least shortening. We reconstructed hanging wall anticlines following the methodology of Suppe (1983).

We made several simplifying assumptions in the construction of our cross section. We assumed that deformation was accommodated by layer-parallel shear, which is a plausible mechanism for folding of bedded limestone rocks. We assumed that volume (and hence area in the plane of the section) was maintained during deformation. We assumed that there was no transport of material (hence area change) in or out of the plane of the section (i.e., plane strain).

We retro-deformed each fault block in our cross section in the structural analysis software Move 2016.1, using the flexural slip unfolding algorithm that models layer parallel shear. For each fault block we selected a template bed that was restored to horizontal by rotation, and then other beds and faults were rotated passively, along with the template bed. This restoration was done relative to a pin line in each fault block, at a point where we expected minimal layer parallel slip. Our restored section is line length and area balanced.

3.4. Palinspastic Reconstruction

We used paleomagnetic and stratigraphic constraints on deformation and the modern dimensions of structural units to build a kinematic restoration of the Central Taurides using GPlates software. As a basis for our reconstruction, we used the restoration of Greece and western Turkey of van Hinsbergen and Schmid (2012), the restoration of central and eastern Turkey of Gürer and van Hinsbergen (2018), of McPhee (2018), and Maffione et al. (2017) and then we incorporated the restoration of Miocene oroclinal bending of the Central Taurides of Koç et al. (2018). Our reconstruction is incorporated into the global plate circuit of Seton et al. (2012) with the updated Miocene Atlantic reconstruction of DeMets et al. (2015). We tested our reconstruction against published paleomagnetic data and our new paleomagnetic data from the Central Taurides. To this end, we computed the Global APWP of Torsvik et al. (2012) in the coordinates of our restored blocks. We used the approach of Li et al. (2017) on paleomagnetism.org (Koymans et al., 2016) to compare our calculated APWP with our in situ data. Our palinspastic reconstruction estimates convergence accommodated across the Taurides fold-thrust belt since the Cretaceous, which we have compared

with our restored minimum shortening from the balanced cross section to constrain the extent of wholesale subduction without accretion (and thus shortening) in the Taurides.

4. Results

4.1. Paleomagnetism

The intensity of the natural remanent magnetization (NRM) of the studied samples is relatively low at five sites (AVD, GUN, IBR, PEM, and SIR), where it ranges between 60 and 6,500 μA/m, and extremely low, between 2 and 35 μA/m, at the remaining two sites (BAS and PIN). Despite these weak NRM intensities, which may be due to a low concentration of ferromagnetic minerals within the carbonate matrix, stable and measurable magnetic remanences are observed in most of the samples (Figure 3a). In a few specimens from sites BAS, PEM, and PIN, no remanence component could be isolated due to the low stability of the remanence.

Two components of magnetization are present in all samples except those from sites PIN and SIR, where predominantly single component remanences commonly associated with high NRM intensities are present (Figure 3a). Magnetization decays progressively during the thermal demagnetization up to the maximum temperature applied at each site (variable between 450 and 580 °C), indicating a wide range of Curie temperatures among the magnetic carriers. This trend is likely produced by the occurrence of different titanomagnetite gains with a variable Ti content. Only few samples from sites AVD and PEM show a rapid decrease of magnetization at 300–350 °C, followed by a progressive decrease up to the maximum applied temperature, which suggests the occurrence of mixtures of titanomagnetite and (likely) iron sulfides.

Where present, secondary (viscous) remanence components were removed at temperatures of 150–180 °C, with higher temperatures (~300 °C) only required by few samples from site AVD (Figure 3a). High-temperature ChRM components were calculated using both anchored best fit lines and great circles and were isolated at around 300–350 °C (sites BAS, PEM, and PIN) as well as at a higher temperature range between 500° and 580 °C (sites AVD, GUN, IBR, and SIR; Figure 3a). Maximum angular deviation values for the isolated ChRMs are below 10° in most of the samples, except those from BAS where they are up to 20°.

Virtual geomagnetic pole distribution is representative of the PSV scatter ($A95_{min} < A95 < A95_{max}$; see Deenen et al., 2011 at all sites except PIN and SIR; Table 1 and Figure 3b). According to Deenen et al. (2011) representation of PSV in a data set may indicate a primary origin of the remanence. VGP scatter from sites PIN and SIR is well beyond that produced by PSV alone (likely due to lightening as suggested by the high NRM intensity and the single component of their remanences), and for this reason, these sites have been discarded from further analysis.

Site mean directions from the remaining five sites show both reversed (four sites) and normal (one site) polarity (Table 1 and Figure 3ci). The distribution of these mean directions is fairly antipodal in tilt corrected coordinates (Figure 3ci), but the result of the reversal test (McFadden & McElhinny, 1990) was indeterminate due to the occurrence of only one normal polarity site. The five tilt-corrected site mean directions are consistently oriented north-eastward when they are transposed to normal polarity (Table 1 and Figure 3ci). This pattern is even more evident when all the ChRM directions from the five sites are plotted altogether and transposed to normal polarity (Table 1 and Figure 3ciii). For this reason we have treated the five sites as belonging to the same population and have calculated 2 mean tilt corrected directions using either the five site mean values ($D/I = 039.0°/33.7°$) or the 48 discrete directions from the five sites ($D/I = 039.2°/32.6°$; Table 1 and Figure 3ciii). In both cases the data scattering resembles that expected from PSV (Table 1), suggesting that the effect of differential rotations between sites, and by inference, across thrust faults within the Geyikdağı nappe, is negligible.

The ChRM directions from all sites are slightly more clustered in tilt corrected than in geographic coordinates (Figure 3ciii) with larger K and smaller A95 values (see Table 1), consistent with a prefolding, likely primary magnetization. However, due to the low variability of the bedding plane orientations in the study area, and the result of the fold test (Tauxe & Watson, 1994) is positive, although with maximum eigenvalues between 51 and 110% unfolding).

Because both the fold test and the reversal test were indeterminate, the primary origin of the remanence in the studied rocks cannot be tested statistically. However, the in situ directions (both site mean values and discrete ChRMs) are significantly different from the present-day geocentrix axial dipole field direction at

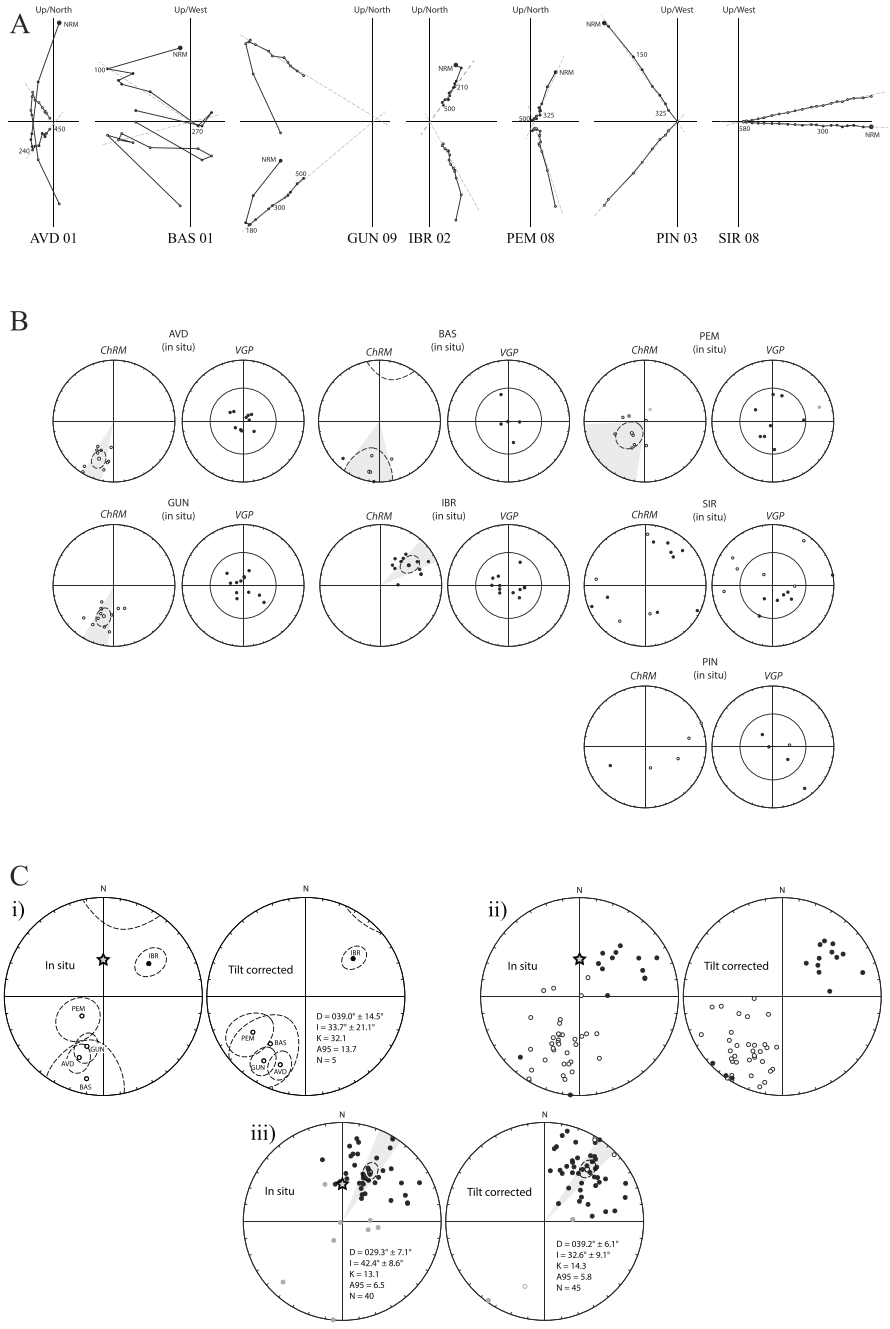

Figure 3. (a) Demagnetization Zijderveld diagrams (Zijderveld, 1967) of one representative sample per site shown in in situ coordinates. The solid and open dots represent projections onto the horizontal and vertical planes, respectively. Demagnetization step values are in °C. The dotted black lines are the best fit lines computed for the ChRMs. (b) Equal area stereographic projections of the in situ co-ordinate characteristic remanent magnetizations (ChRMs) and associated virtual geomagnetic poles (VGPs) for the studied sites from the western central Taurides. The full and open dots in the ChRM plots indicate normal and reverse polarity, respectively. The larger dots in (ii) and (iii), the dotted ellipses, and the gray shaded areas indicate the site mean values, their 95% cones of confidence, and the uncertainty on declination (dDx), respectively. The smaller circles in the VGP plots indicate the extent of the 45° cutoff (Johnson et al., 2008) applied to the VGPs before computing the mean values. (c) Equal area stereographic projections of the in situ and tilt corrected (i) site mean directions and associated 95% cone of confidences and (ii and iii) ChRM directions from sites IBR, PEM, GUN, AVD, and BAS. (iii) ChRM directions transposed to normal polarity. The gray dots are the ChRM directions rejected after the 45° cutoff (Johnson et al., 2008). The full and open dots indicate normal and reverse polarity, respectively. The gray star is the present-day geocentrix axial dipole (GAD) field direction at the latitude of the study area. The larger dots in (ii) and (iii), the dotted ellipses, and the gray shaded areas indicate the site mean values, their 95% cones of confidence, and the uncertainty on declination (dDx), respectively. Mean tilt corrected directions for the study area in the western central Taurides are shown in (i) and (iii) (see also Table 1).

Table 1
Paleomagnetic Results From the Western Taurides (Turkey)

					In situ				Tilt corrected							
Site	Lat (°)	Long (°)	N	N45	D	ΔD_x	I	ΔI_x	D	ΔD_x	I	ΔI_x	K	A_{95}	A_{95min}	A_{95max}
AVD	37.2635	32.3209	10	10	201.6	9.7	−34.1	14.1	200.6	8.9	−27.3	14.5	32.3	8.6	4.8	19.2
BAS	37.3716	31.3919	5	5	191.5	25.2	−16.3	46.9	216.8	28.9	−40.0	36.4	9.3	26.4	6.3	29.7
GUN	36.8854	32.1302	12	12	198.2	12.5	−45.9	13.6	213.2	8.8	−23.4	15.2	26.4	8.6	4.4	17.1
IBR	37.1318	31.5637	12	12	54.2	12.9	42.8	15.3	51.3	9.5	38.8	12.4	25.1	8.8	4.4	17.1
PEM	36.8351	32.0920	9	8	227.7	39.2	−66.1	18.5	236.0	17.2	−35.7	24.1	11.1	16.2	5.0	20.5
PIN*	37.3714	31.4378	5	0	-	-	-	-	-	-	-	-	-	-	-	-
SIR*	37.9806	31.0661	13	0	-	-	-	-	-	-	-	-	-	-	-	-
All sites (directions)			48	40	29.3	7.1	42.4	8.6	-	-	-	-	13.1	6.5	2.6	7.5
All sites (directions)			48	45	-	-	-	-	39.2	6.1	32.6	9.1	14.3	5.8	2.6	7.5
All sites (site averages)			5	5	-	-	-	-	39.0		33.7		33.5#	13.4#		

Note. For the locality average based on site averages, *k* and α95 were calculated assuming Fisherian distribution of site-average directions (see Deenen et al., 2011).

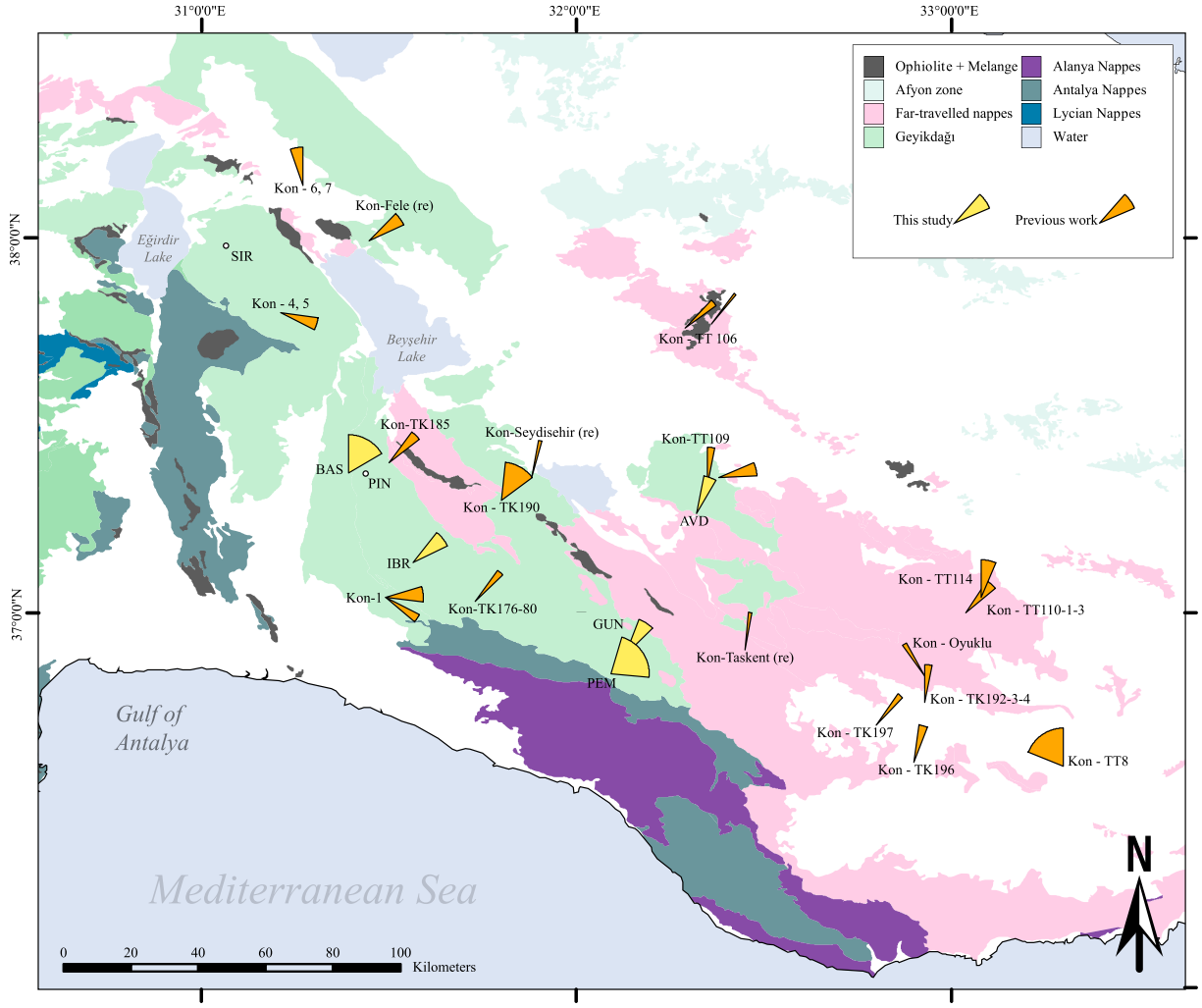

Figure 4. Paleomagnetic rotations in the western central Taurides from this study and a compilation of data from Kissel et al. (1993), Meijers et al. (2011), and Cinku et al. (2016; available in supplementary file DS01). Rotation "cones" reflect ΔDx (uncertainty). Sites PIN and SIR are indicated on the map as points. The abbreviation "(re)" indicates sites in which rotations were measured in remagnetized rocks.

the average latitude of the study area, calculated as $D/I = 000°/56.5°$ (Figure 3c), and recent remagnetization is therefore excluded. Furthermore, the paleolatitude of the studied rocks calculated using the mean value of $D = 039.2° \pm 6.1°$, $I = 32.6° \pm 9.1$ obtained from all the discrete directions (see Table 1) matches precisely the expected paleolatitude for the stable African plate in the Eocene according to the apparent polar wander path (APWP) of Torsvik et al. (2012; Figure 3di). This provides more robust evidence for the primary origin of the remanence of the studies rocks (Figure 4).

4.2. Fault Kinematic Results

We collected fault slip data from 22 sites across the western Central Taurides (Figure 5). Of those, six sites had sufficient (i.e., ≥10) compatible fault slip data for paleostress inversion (Figure 6). The sample size is somewhat limited in terms of the number of fault slip data measured, and the number of sites collected (i.e., we may undersample some groups of fault slip data), and so we merely use our results to evaluate whether fault slip on thrusts is essentially parallel to our line of section.

Many of the thrust fault zones we measured contain an apparently subordinate group of fault slip data consistent with a phase of oblique or strike-slip motion, although we do not see an overall trend in the sense of slip in these data from site to site. At some sites, we also see evidence for changing kinematics on the same fault plane (e.g., sites PIN and AKC).

We find sites that contain evidence for a single phase of dip-slip thrusting (e.g., sites YAY and MR1) and sites with multiple incompatible phases of thrusting (e.g., sites URU and UZU). In the northwest part of the belt, thrust fault zones consistently contain fault slip data consistent with a phase of westward transport, whereas in the southeast part of the belt, thrust faults contain fault slip data consistent with a phase of southward to south-westward transport. These transport directions closely follow trends of mapped thrust faults and associated fold axes (Figure 5), which form a SW-convex orocline. We did not find well-exposed fault zones in the Başgölcűk thrust, or associated with the Kirkavak ridge, and so we measured fold axes to infer transport direction. In both sites, folding indicated a westward transport direction, consistent with fault slip data collected in structurally higher thrust faults (i.e., MR1 and PIN).

A series of steep SE-NW-trending strike-parallel faults between Seydişehir and Hadim form a major fault zone, which cuts through the Gündoğmuş-Hadim section line. This fault zone cross cuts thrust faults and folds in the Aladağ and Bolkardağı nappes and therefore postdates Eocene thrusting in the belt. Vertical displacements greater than 1–2 km are evident in many places (e.g., along the Gündoğmuş-Hadim section line). The Hadim fault cross cuts and displaces a limb of a noncylindrical fold in the Aladağ nappe, weakly constraining ~5-km right-lateral strike-slip offset (Figures 6viii and 7a).

We found evidence for phases of normal faulting and right-lateral strike-slip kinematics in those fault zones. These are likely a result of reactivation, although we did not find strong evidence for relative timing of each fault set.

4.3. Cross-Section Observations and Interpretations

We present our field data on a small-scale strip map in Figure 6, which is accompanied by a description of our field observations in Table 2, and photographs of key field relationships in Figure 7. Using these data, we construct a cross section from Gündoğmuş to Hadim (Figure 8), in which we find evidence for a minimum of 27-km shortening on thrusts within the Geyikdağı nappe, a minimum of 70-km shortening by thrusting of the Aladağ and Bolkardağı nappes over the Geyikdağı nappe, and a minimum of 57-km shortening by thrusting of the Bozkır nappes over the Aladağ and Bolkardağı nappe. In total, we find a minimum of 154 km of shortening along our cross section of the Central Taurides. Our cross section is not strictly balanced because our assumption of plane strain is violated by the Hadim strike-slip fault. However, folding on the northern side of the Hadim fault is cylindrical to the first order (i.e., on the scale of the strike-slip displacement) and so structures to the north and south of the Hadim fault should match up.

Orogen-scale cross sections are ideally balanced relative to an undeformed foreland (Woodward et al., 1989). In our new cross section, the Alanya and Antalya nappes likely cover the foreland. The thickness of those nappes, and therefore the depth to the top of the foreland, is not directly measurable, and so we instead use the amplitude of the Pembelik monocline to estimate the depth of the foreland.

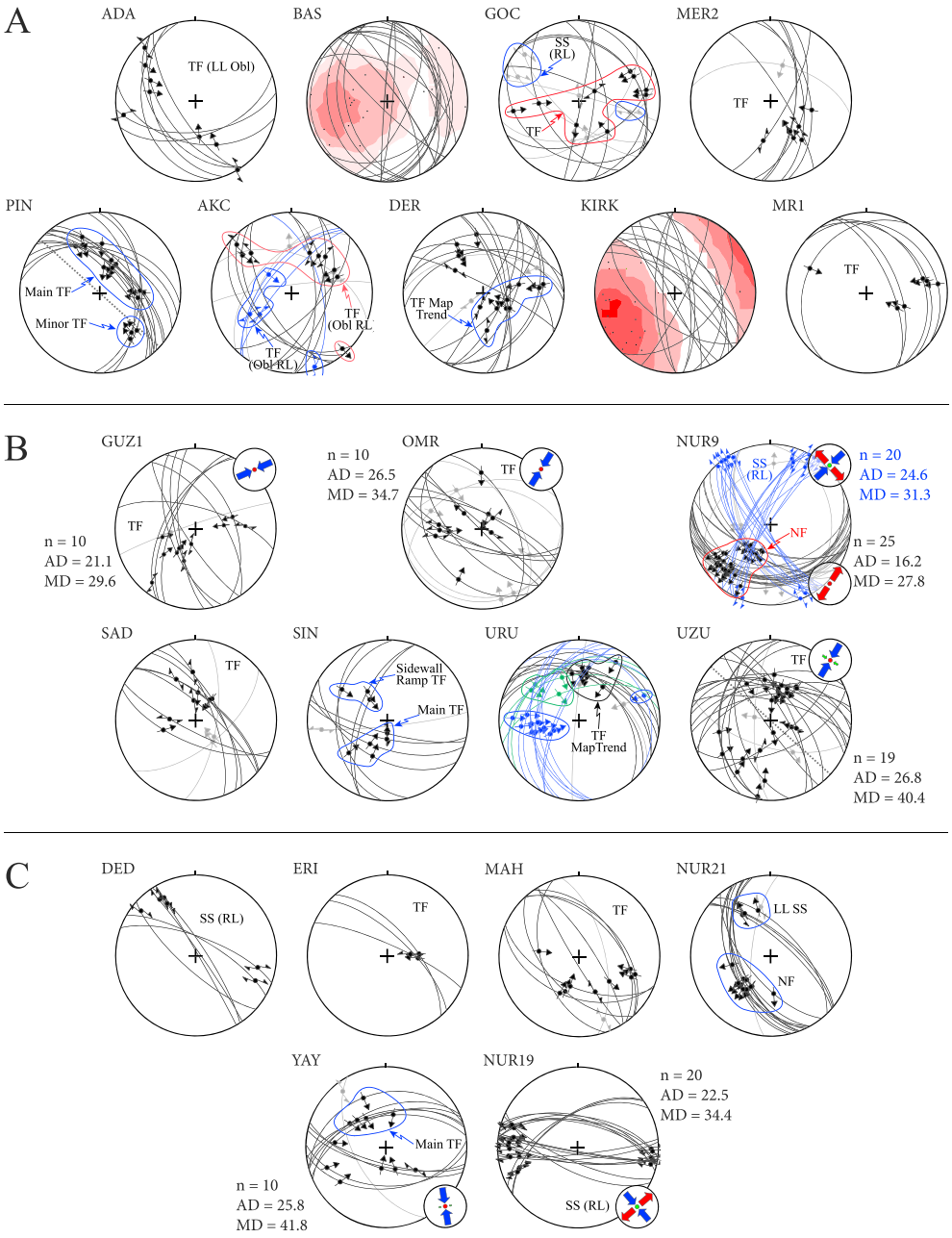

Figure 5. (a) Site location map of fault kinematic data collected across the western central Taurides, showing fold axes and faults. (b) Angelier plots of kinematic data collected across the western central Taurides separated by region. The light gray great circles represent incompatible (outlying) kinematic data. Abbreviations NF, SS, and TF are normal fault, strike-slip fault, and thrust fault, respectively. LL, RL, and Obl are left lateral, right lateral, and oblique, respectively. Supplementary file 01 contains a table of our fault kinematic data. (i) The northern area. Sites BAS and KIRK are fold axes measured from meter-scale folds. (ii) The central area. (iii) The southern area of the western central Taurides. Paleostress inversion was conducted on six sites in WinTensor software (Delvaux & Sperner, 2003). Fault-slip data were converted to *P*–*T* axes and then separated into compatible kinematic populations. AD, MD, and n are average angular deviation from the calculated inversion, maximum angular deviation from the calculated inversion, and number of data used in the inversion, respectively.

The well-exposed Geyikdağı thrust fault imbricate forms the high ridge of the Taurides range and contains a deformed sequence of Geyikdağı nappe rocks. The thrust fault imbricate is not deeply eroded and contains preserved hanging wall anticlines, which are a strong constraint on our structural model and limit the amount of shortening that can be accommodated by thrusting in the Geyikdağı nappe. However, a lack of deep

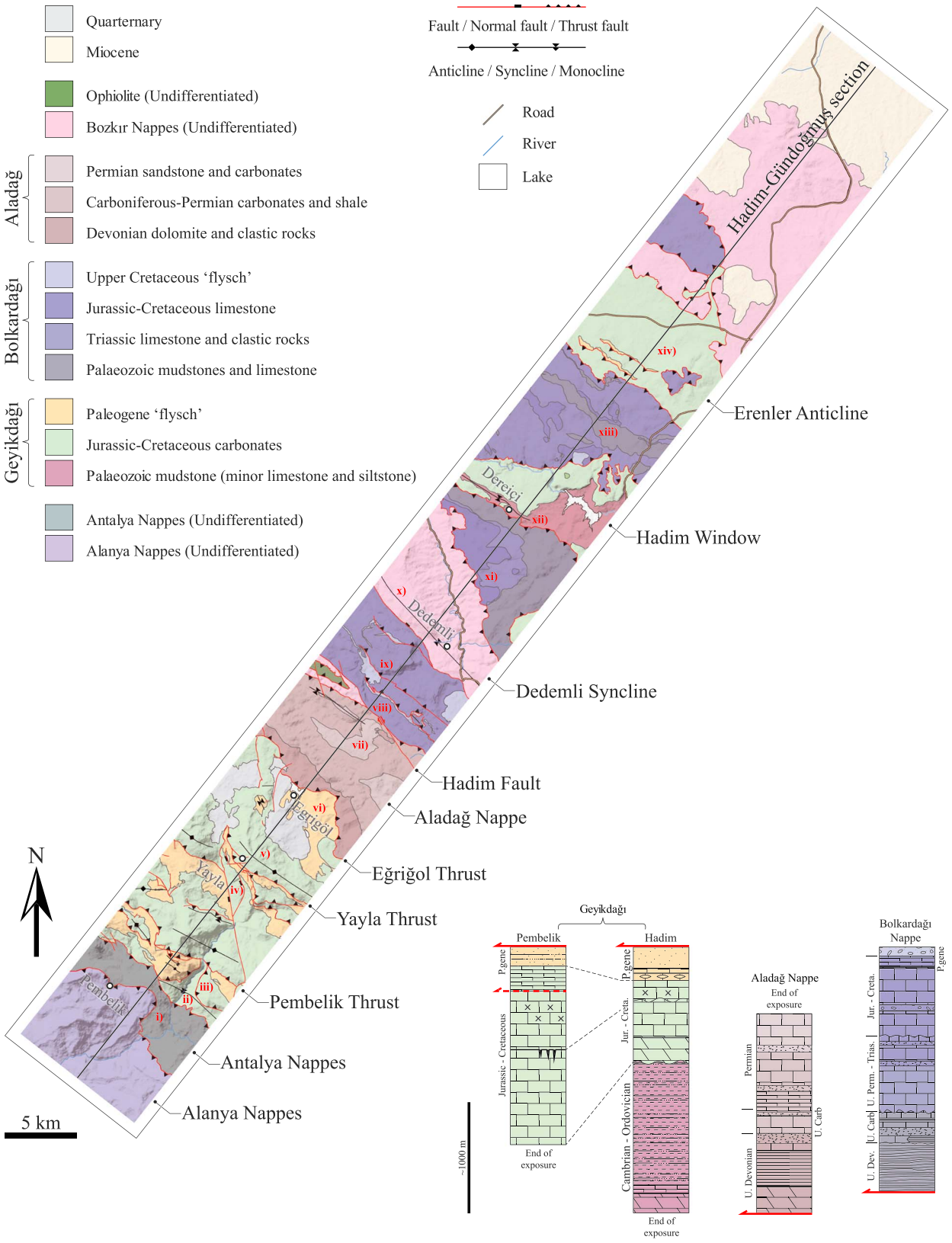

Figure 6. Our 10-km-wide strip map along the Gündoğmuş-Hadim section line showing generalized stratigraphy and major structures and a simplified stratigraphic scheme of the rocks exposed within the strip map. The dip data are available on a large scale map in supplementary file 01. Descriptions in Table 2 are demarked by red roman numerals. Note that on some fault contacts, exposures of Eocene flysch were too small to include on the map.

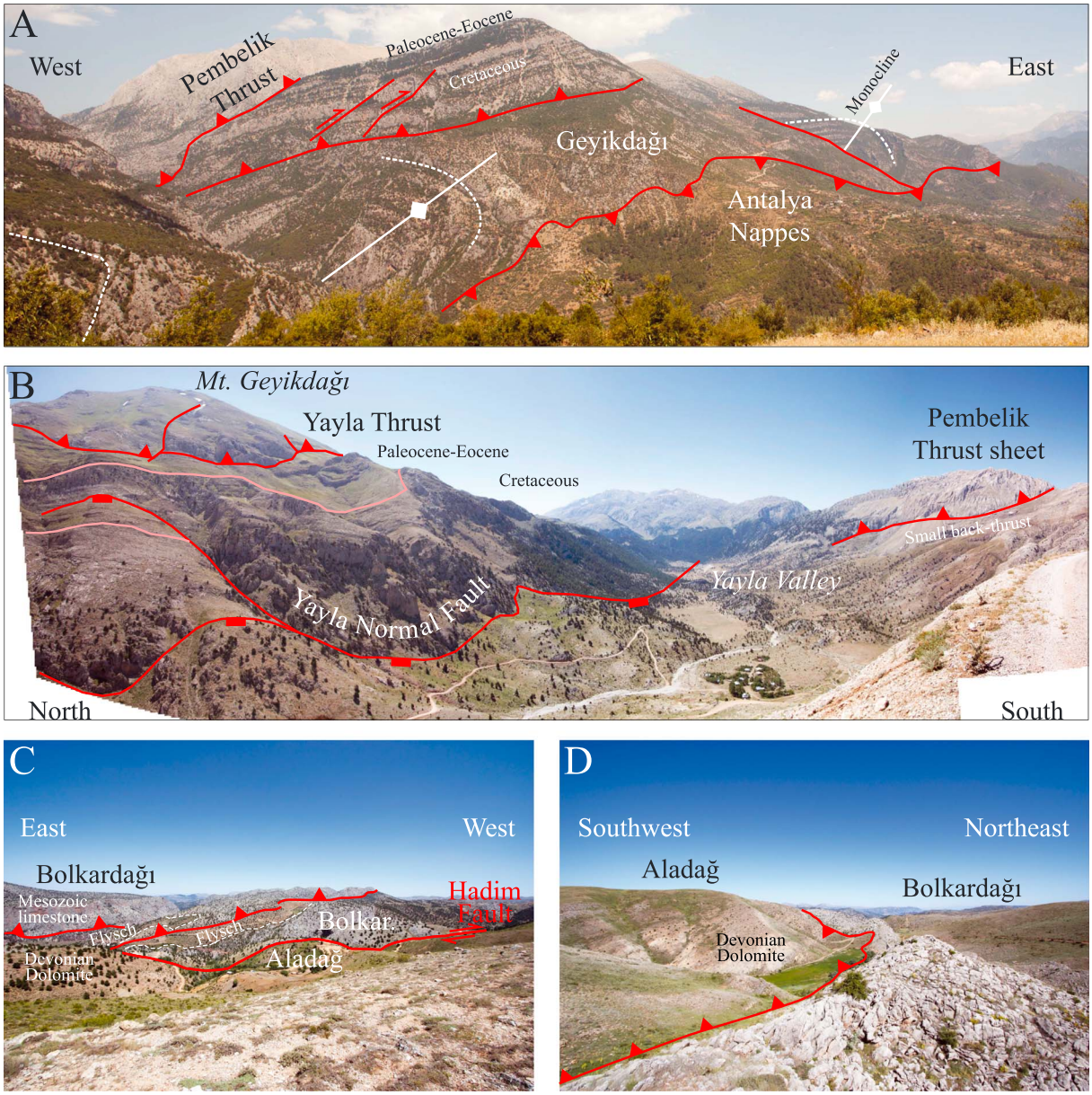

Figure 7. Photographs of key field relationships along the Gündoğmuş-Hadim section, which are described in Table 2. (a) Pembelik monocline in the foreground, midground and background, and its relationship with the Pembelik thrust faults. (b) Mt. Geyikdağı with the Yayla normal fault and the Yayla thrust fault above. The Paleocene-Eocene sediments below the Yayla thrust fault are internally deformed, but we omitted our interpretation for clarity. (c) In the foreground, the Hadim fault separates the Aladağ and Bolkardağı nappes, near Dedemli. In the background, thrust faulting of Mesozoic limestone over Upper Cretaceous flysch within the Bolkardağı nappe. (d) Devonian dolomite of the Aladağ nappe back thrusting over the Bolkardağı nappe.

erosion also means that lower structural levels have not been exhumed, creating uncertainty in the style of subsurface structures. We therefore use steep back-dipping dip domains to constrain the position of thrust ramps in the subsurface.

Thin skinned fold-thrust belts evolve above a shallow dipping planar décollement (e.g., Davis et al., 1983). In the southwest part of the strip-map, below the Yayla and Pembelik thrusts, we use the observed thickness of the thrust sheets to estimate the depth to décollement, and find that a 3°NE-dipping décollement best accommodates the surface structures. This is within the typical range of décollement dips reported for thin-skinned fold-thrust belts.

Table 2
Descriptions of Key Field Relationships From Southwest to Northeast Along the Gündoğmuş-Hadim Section Line

Location	Description
Antalya-Alanya nappes i) (A)	The Alanya nappes form a continuous cover from the Mediterranean coast to the edge of the Geyikdağı mountain range. The internal structure of these nappes is poorly known and was formed by at least one pre-middle Eocene deformation phase, which is demonstrated by Eocene limestones that unconformably cover thrusting and folding in the Antalya-Alanya nappes (Özgül, 1984).
Pembelik monocline ii) (A)	A ~1-km-high SW dipping limb of a monocline forms the steep edge of the Geyikdağı mountain range and can be traced for tens of km along strike. This folded the overlying Alanya nappes and exposed a narrow band of the underlying Antalya nappes ("Alakırçay" nappe of Özgül, 1976), which appears to be only a few hundred meters thick and remains very thin for tens of km along strike. On the section line, the flat-on-flat contact between the Alanya-Antalya nappes is cut by a steep normal fault.
Pembelik thrusts iii)	The eastern limb of the monocline dips shallowly NE and contains a 100- to 200-m-thick sequence of Upper Cretaceous to Eocene carbonate and clastic rocks. Those rocks are deformed into a tight thrust imbricate that also incorporates the upper ~100 m of underlying platform carbonates. The thrust faults sole into a shallow, NE-dipping flat-on-flat thrust that cuts straight through the SW dipping limb of the monocline. The thrust imbricate abuts against overthrusted Upper Cretaceous platform rocks along an ~60°NE dipping thrust fault. The overlying thrust sheet was inaccessible due to steep terrain, and so our mapping is based on observations from a distance, but in general, the thrust sheet forms a NW-SE trending anticline.
Yayla normal fault iv) (B)	The east side of the Yayla valley is bound by a steep, ~0.5-km-high scarp of Upper Cretaceous limestone. The juxtaposition of the Upper Cretaceous platform rocks with Upper Cretaceous-Eocene clastic bearing rocks is locally ambiguous, but toward the north, along the valley side, a conspicuous, ~45°SW dipping normal fault is visible, as well as minor normal faults which are strike parallel to the modern erosional scarp. The top of the Yayla normal fault scarp is marked by an ~50–m-thick sequence of the Upper Cretaceous-Eocene clastic rocks that have the same dip as those in the footwall of the normal fault.
Yayla thrust fault v) (B)	Upper Cretaceous rocks have been thrusted on top of Eocene rocks at the top of the Yayla fault scarp. The overlying thrust sheet contains SW dipping beds of pink Upper Cretaceous limestone that form a hanging wall anticline. The hanging wall anticline and underlying thrust are cut at an oblique angle by the steep Yayla normal fault that displaces the fold axis westward across the valley. Nearby, Eocene rocks in the footwall of the thrust are exposed in a reentrant in the thrust contact. Those Eocene rocks constrain a minimum displacement on the Yayla thrust fault, and a footwall dip of ~20°E indicates an underlying thrust ramp. The shape of the eastern side of the Yayla thrust sheet is poorly constrained as the limestones there are massive, and the rocks have been deeply eroded by glacial valleys, and then covered by thick glacial moraine.
Erigöl area vi)	The Erigöl area has a much lower relief than the Geyikdağı range. A thick sequence of Eocene *flysch* and underlying Upper Cretaceous carbonates are exposed between superficial ridges of glacial moraine and klippen of Aladağ nappe rocks. The wide outcrop of Eocene rocks suggests that the underlying Geyikdağı platform rocks dip shallowly E, before plunging below a continuous ridge of Aladağ nappe rocks.
Aladağ nappe vii)	The lowermost stratigraphy of the Aladağ nappe consists of intensely deformed Devonian to Carboniferous clastic rocks. Those are overlain by a high relief ridge of internally deformed well-bedded limestone, which dips steeply E, indicating the position of an underlying thrust ramp in the Geyikdağı platform. Further to the northwest, the dips become shallow and then steepen to define a tight syncline that contains Permian clastic rocks. The west dipping limb of that syncline is cut by the Hadim Fault.
Hadim fault zone viii) (C & D)	The Hadim Fault places the Aladağ nappe next to faulted blocks of the Bolkardağı nappe. The fault cuts through and displaces a strongly noncylindrical syncline in the Aladağ nappe and defines a lateral displacement of up to ~7 km. Immediately to the northwest of the section line, the syncline in the Aladağ nappe is well preserved and contains a W dipping limb that steepens and overturns. A subvertical out of sequence thrust fault, or normal fault, places the Aladağ nappe next to an ophiolite block. The Hadim fault bounds the eastern edge of the ophiolite, obscuring the original relationship of the ophiolite and Bolkardağı nappes there. Further to the west along the Hadim fault, the original contact between the Aladağ nappe and Bolkardağı nappe is preserved, where Aladağ nappe has been thrust NE over the Bolkardağı nappe.
Bolkardağı nappe (Dedemli) ix)	The Bolkardağı nappe contains an Upper Cretaceous *flysch*, a Mesozoic carbonate sequence, and a Paleozoic mixed clastic and carbonate sequence. Those rocks are affected by intense small scale (i.e., below the resolution of our study) folding and faulting, and on a larger scale, are cut by a series of thrust faults that thrusted the Mesozoic carbonate sequence onto the Upper Cretaceous *Flysch*.
Dedemli syncline x)	A poorly exposed normal fault places the Bolkardağı nappe next to a klippe of the Bozkır nappes. An internal nappe from high in the tectonostratigraphy of the Bozkır nappes (see Andrew & Robertson, 2002) is preserved on the klippe and defines a NW-SE trending syncline.
Bolkardağı nappe (Söğüt) xi)	The Bolkardağı nappe reappears below the eastern limb of the Dedemli syncline and consists mostly of poorly exposed Triassic to Devonian clastic and carbonate rocks, which are affected by noncylindrical mesoscale folding. The northeastern edge of the Bolkardağı nappe is bound by a tectonic window that exposes the underlying Geyikdağı rocks.

Table 2 *(continued)*

Location	Description
Hadim window xii)	A flat-on-flat thrust contact separates Devonian shale of the Bolkardağı nappe from underlying Jurassic-Cretaceous limestone of the Geyikdağı platform. The limestone is extremely thin (~200 m) compared to the sequence at Yayla and Pembelik. At the village of Dereiçi, the Jurassic-Cretaceous limestone is absent, and underlying Cambro-Ordovician shales are in direct contact with the Bolkardağı nappe. The window is ~200 m wide at Dereiçi but widens to 5 km to the southeast near Hadim. The window defines an open anticline that corresponds roughly to the Seydişehir anticline of McPhee et al. (2018). To the northwest of the section, the Bolkardağı nappe is absent, and the Bozkır nappes are in direct contact with the Geyikdağı platform. The northeastern edge of the window is bound by another klippe of the Bolkardağı nappe that contains Upper Cretaceous to Jurassic carbonates that dip S onto the underlying Geyikdağı as a hanging wall anticline.
Bolkardağı nappe (Yelbeyi) xiii)	The exposed Bolkardağı nappe again consists of a poorly exposed Triassic to Devonian mixed sequence of clastic and carbonate rocks that are intensely affected by noncylindrical mesoscale folding and thrust faults that verge in both a NE and SW sense. The internal deformation made it difficult to take reliable bedding measurements, and poor exposure meant that detailed mapping of the Bolkardağı nappe was beyond the scope of this work.
Erenler anticline xiv)	The most northerly exposure of the Geyikdağı platform is exposed in a tectonic window as a wide, open anticline which runs NW-SE for ~50 km. Again, both Bozkır and Bolkardağı nappes are in contact with the Geyikdağı along the window. This window marks the minimum extent of overthrusting of the Aladağ, Bolkardağı, and Bozkır nappes over the Geyikdağı rocks.

Note. Numeral codes refer to points on the strip map (Figure 5), and the cross section (Figure 7A). Letter codes refer to photographs on Figure 6.

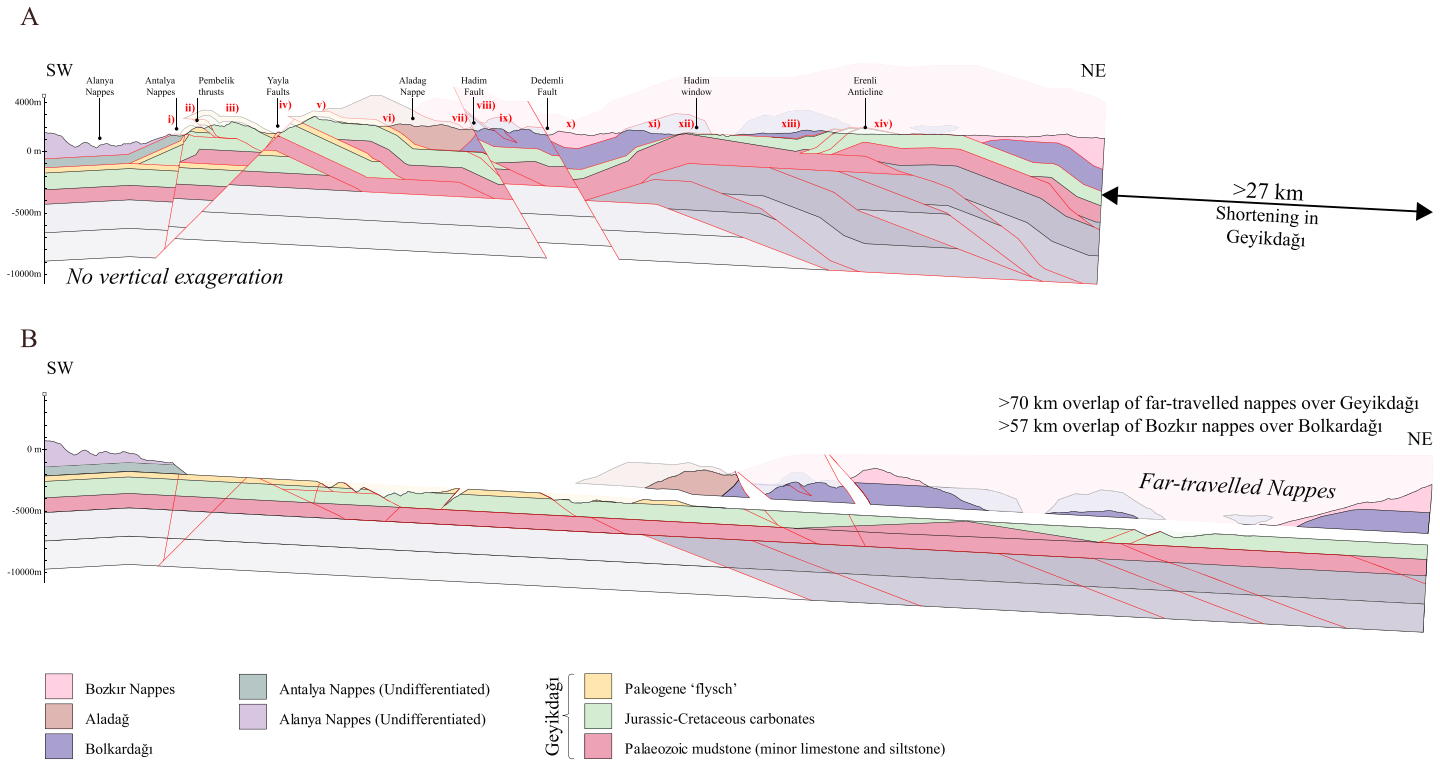

Figure 8. (a) The Gündoğmuş-Hadim balanced cross section, with a generalized internal stratigraphy within the far-traveled nappes. A large-scale version of this figure is available in supplementary file 01, and shows dip data that we used to construct the cross section. (b) Retro-deformed cross section at the same scale as the deformed section.

In the northeast part of strip-map, the far-traveled Aladağ, Bolkardağı, and Bozkır nappes cover Geyikdağı nappe rocks that are exposed in a series of tectonic windows. Those windows are bound to the northeast and southwest by synclines, defining a regional-scale anticline in the underlying Geyikdağı nappe. In the absence of evidence for significant thrusting of the upper few kilometers of Geyikdağı nappe rocks there, we interpret that as an anticline that enveloped a thrust duplex in the underlying Paleozoic Geyikdağı stratigraphy. Thick thrust sheets are required to fill space below the anticline while balancing the thrusting toward the foreland, and so we interpret that the décollement steps down, deep into the Geyikdağı nappe stratigraphy. This interpretation minimizes shortening, as well as structural complexity, and is structurally compatible with the Bucak-Seydişehir section to the north (Figure 1c). The flat-on-flat thrust contact between the far-traveled nappes and Geyikdağı nappe rocks suggests the far-traveled nappes were likely emplaced before internal thrusting started to imbricate the Geyikdağı nappe.

In contrast to the Beyşehir-Beydağları section to the north (McPhee et al., 2018), we find no evidence for Miocene thrusting. Instead, our structural analysis suggests that the emergent parts of the southern Central Taurides were undergoing extension, most likely in the Miocene.

5. Discussion

5.1. Palinspastic Reconstruction

Our three independent data sets point to a coherent vertical axis rotation of the Geyikdağı nappe since middle Eocene times. Our first data set consists of paleomagnetic data, which we collected to verify whether the Geyikdağı nappe rotated as a coherent domain despite diffuse internal thrusting. We find no evidence for differential rotations between adjacent thrust sheets within the Geyikdağı nappe. Our new paleomagnetic data confirm previous work from the Taurides (Cinku et al., 2016; Kissel et al., 1993; Meijers et al., 2011; Piper et al., 2002) in that the Geyikdağı nappe underwent a post-middle Eocene vertical axis rotation of ~40° relative to the geocentric axial dipole (Table 1). The area affected by a rigid block rotation is $>$100 km long from northwest to southeast. Structural trends of thrust faults and fold axes suggest that the rotated domain is up to about 175 km long from the Isparta angle in the far northwest to the Central Taurides. In our reconstruction, we therefore treat the Geyikdağı nappe as an internally shortened, but coherent domain affected by an ~40° CW rotation since the middle Eocene.

The absence of extension to the north and east of the Geyikdağı nappe in middle Eocene to early Miocene time means that rotation of the Geyikdağı nappe required a lateral gradient in shortening. To assess the magnitude of that shortening, we developed a palinspastic reconstruction (Figure 9a). We first reconstruct up to 300 km of convergence between the western end of the Geyikdağı nappe and the Aladağ nappe and 90 km between the eastern end of the Geyikdağı nappe and the Aladağ nappe. As well as Africa-Eurasia convergence, this includes an additional 100–130 km of convergence between Africa and Central Anatolia reconstructed by Gürer and van Hinsbergen (2018). Previous kinematic reconstructions of western Anatolia (van Hinsbergen et al., 2010) suggested that the Beydağları platform accreted to the upper plate at ~35 Ma (van Hinsbergen et al., 2010; van Hinsbergen & Schmid, 2012). We assume that the western part of the Geyikdağı nappe moved together with the Beydağları platform until that time. We assume that the eastern end of the Geyikdağı nappe accreted to the upper plate at ~42 Ma in accordance with the youngest stratigraphic ages of the Geyikdağı nappe. This reconstruction sequence alone leads to northward increasing shortening (up to ~160 km) above the Geyikdağı nappe, and southward increasing shortening below the Geyikdağı nappe (up to ~160 km). This diachronous accretion predicts a CW rotation that fits well with the paleomagnetic data (Figure 9b) and is kinematically feasible given stratigraphic and paleomagnetic constraints. After accretion of Beydağları to the upper plate at 35 Ma, the Taurides are restored as part of Central Anatolia (Gürer & van Hinsbergen, 2018). Finally, the Taurides are affected by Miocene rotations as documented by Koç et al. (2018).

Our estimates of convergence are subject to uncertainty. The error bars associated with Africa-Europe convergence are on the order of tens of kilometers (e.g., van Hinsbergen & Schmid, 2012). Shortening estimates within Central Anatolia rely on paleomagnetic constrains on the magnitude of rotations and structural constraints on the size of rotating domains (van Hinsbergen et al., 2018; Gürer & van Hinsbergen, 2018), leading to uncertainty of several tens of kilometers. Finally, the ages of accretion and end of sedimentation within nappes may be several million years younger or older due to biostratigraphic uncertainty, corresponding

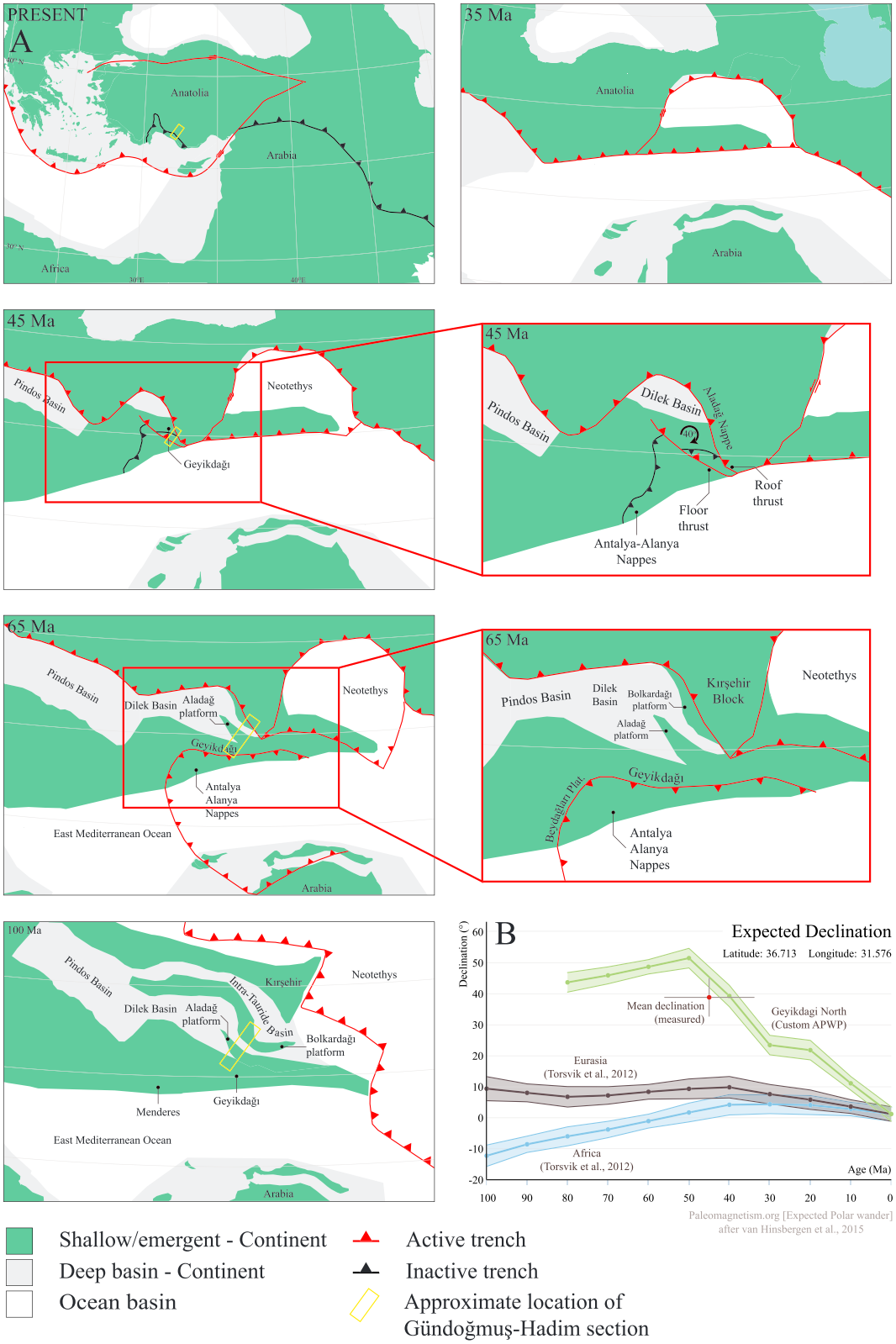

Figure 9. (a) Palinspastic map view reconstruction of the Taurides since 100 Ma. Restoration of eastern Turkey follows Gürer and van Hinsbergen (2018), of intraoceanic subduction follows Maffione et al., 2017, and for Greece and western Turkey follows van Hinsbergen and Schmid (2012) and Gaina et al. (2013). (b) Comparison of mean declination for paleomagnetic data in the Geyikdağı nappe, with calculated APWPs for Africa, Eurasia from Torsvik et al. (2012), and Geyikdağı nappe calculated from our reconstruction.

to tens of kilometers of convergence uncertainty. Although it is hard to estimate precisely, the convergence estimate may be associated with a ±100-km uncertainty.

We used seismic tomographic images of the mantle below Turkey to test whether the large area consumed by convergence in our palinspastic reconstruction is reliable. The Eocene age fold-thrust belt (and hence the "trench") did not propagate through the Beydağları foreland, meaning that Africa-Europe convergence after Eocene times was no longer accommodated in the Central Taurides (McPhee et al., 2018). Mantle tomography (Biryol et al., 2011; van der Meer et al., 2018) and earthquake hypocenters (Kalyoncuoğlu et al., 2011) show that the Beydağları foreland is currently underlain by the "Antalya slab" (Biryol et al., 2011; van der Meer et al., 2018), which may contain the subducted lithospheric underpinnings of the Taurides that became isolated from African lithosphere upon Eocene accretion of Beydağları to Anatolia (McPhee et al., 2018). In contrast to the northwestern part of the belt, oceanic lithosphere was likely subducting below the southern margin of the Central Taurides fold-thrust belt (e.g., McPhee, 2018; Barrier & Vrielynck, 2008). Subduction there remains active today and is represented by the Cyprus slab (Biryol et al., 2011; van der Meer et al., 2018). An along-strike change in the type of subducted lithosphere, from oceanic in the southeast, to continental in the northwest, may have formed a vertical tear that is interpreted between the "Cyprus slab," and "Antalya slab" in mantle tomography of the region (Biryol et al., 2011). Hence, the large Paleocene to Eocene convergence estimates accommodated within the Taurides may be surprising in the light of the estimates of shortening (Figure 8, McPhee et al., 2018) but are not problematic in the light of seismic tomographic images of the mantle below Anatolia.

5.2. Shortening and Wholesale Underthrusting Within the Taurides

We now compare the estimates of convergence with the modern architecture of the Taurides fold-thrust belt and the associated minimum shortening estimates using our new cross section (Figures 7a and 7b) and previously published Bucak-Seydişehir section (Figure 1c, McPhee et al., 2018). We tested for along-strike cylindricity within the Geyikdağı nappe and attempted to identify thrust faults that may have accommodated the CW rotation of the Geyikdağı nappe.

In constructing our cross section we made several assumptions and interpretations that led to uncertainties in our shortening estimate. First, we did not aim to assess Eocene shortening contained in the Paleocene Antalya-Alanya nappes. We may therefore underestimate some post-middle Eocene shortening there, although given that the Alanya nappes form a coherent cover over the underlying Antalya nappes, we may rule out large scale folding and thrusting. We interpret a shallow dipping décollement, based on structural style of the belt, as described by McPhee et al. (2018). Deformation measured at the surface is best reconstructed using a 3° décollement—a steeper or deeper décollement requires more shortening or thicker thrust sheets. In the northeast part of the belt, we observed a regional scale anticline in the Geyikdağı nappe. We reconstruct this as an anticline that envelops a thrust duplex and assume no thrusting cuts the upper few kilometers of Geyikdağı nappe stratigraphy. If this assumption is invalid, we may underestimate shortening in the Geyikdağı nappe by a few kilometers. Taking these uncertainties into account, we conclude that the amount of shortening within the Geyikdağı nappe was probably not much higher than estimated here.

Overall, the structural style that we interpret in the Gündoğmuş-Hadim cross section is cylindrical with that of the Derebucak thrust imbricate and Seydişehir thrust duplex in the Bucak-Seydişehir cross section (Figure 1c, McPhee et al., 2018). Some of the main thrust faults may be continuous with those in the Derebucak thrust imbricate. The Dedemli syncline and Hadim-Erenler anticline seem to be the along-strike continuation of the Huğlu syncline and Seydişehir anticline, respectively (Figure 1c). We find that there may be ~10 km more shortening accommodated by thrusting in the Geyikdağı nappe in the Gündoğmuş-Hadim section compared to the Bucak-Seydişehir section. The far-traveled Aladağ, Bolkardağı, and Bozkır nappes are more extensively exposed in the Gündoğmuş-Hadim section than in the Bucak-Seydişehir section, and so we constrain much greater shortening by thrusting of those nappes (70 km) than is possible to the north (50 km). We note that both are minimum estimates, and the difference does not reflect differences in shortening, but differences in exposure.

The cylindrical architecture of the belt may be reflected in a group of dip-slip fault slip data that record a phase of westward and southwest to southward thrusting, as well as in strike-parallel first-order fold axes and thrust faults, and in paleomagnetic data that demonstrate rotation of a coherent block. Oblique and

strike-slip fault slip data may show a combination of shortening at an oblique angle to N-S Africa-Eurasia convergence during or shortly after rotation of the block or may record the accommodation of Miocene oroclinal bending, which was decoupled from the hinterland part of the belt.

Our analysis reveals that shortening within the Geyikdağı nappe was far too small to have significantly contributed to accommodating the CW rotation. This rotation must instead have been accommodated by a strain gradient on faults surrounding the rotated block. The only structures with displacements large enough to accommodate the rotation are the enveloping basal thrust fault below the duplex and the roof thrust fault below the Aladağ and higher nappes.

The thrust fault at the base of the Aladağ nappe is a likely candidate to for the roof thrust that accommodated up to ~160-km convergence associated with rotation of the Geyikdağı nappe (Figure 9a) because there is a gap between accretion of the Aladağ nappe in Late Cretaceous times and its emplacement onto the Geyikdağı nappe in middle Eocene time. The only accreted remnants of lithosphere that underthrusted the belt in that time interval are thin, thrusted slithers of deepwater basin sedimentary rocks of Dipsiz Göl (Özgül, 1984; Mackintosh & Robertson, 2013). Those rocks may record underthrusting of a basin (likely continent floored) below the Aladağ nappe, prior to thrusting of the Aladağ nappe over the Geyikdağı nappes.

Our palinspastic reconstruction restores a triangle-shaped underthrusted lithospheric region that we infer widens to the northwest and may connect to the restored deepwater basin preserved as the Dilek nappe in western Turkey and Pindos Basin in Greece (Ring et al., 2007; van Hinsbergen et al., 2010; Figure 9). No relics of the Dilek nappe have been found so far in the Lycian Nappes. These make up the west-Anatolian equivalent of the Taurides, illustrating that the Dilek nappe underwent wholesale under-thrusting, comparable to the history we infer for the Central Taurides. Also, deeper tectonic nappes of the Menderes nappes (Gessner et al., 2001), where stacking was time equivalent to the accretion of the Central Taurides (van Hinsbergen et al., 2010), still contain most if not all of their stratigraphic sequence (e.g., Ozer & Sozbilir, 2003), which suggests that they were intact after underthrusting a foreland fold-thrust belt represented by the Lycian Nappes (Figure 1). The Menderes nappes thus demonstrate that wholesale underthrusting beyond the foreland fold-thrust belt is a viable mechanism during Tauride orogeny. We predict a north-westward increase in shortening on the roof thrust from the rotation pole in the southeast of the Taurides. This would have been complimented by a south-eastward increase in shortening on a floor thrust, from the northwest end of the rotated block.

The floor thrust below the rotated Geyikdağı nappe is hard to place with confidence. A ~40° CW rotation must have resulted in differential shortening of many tens of kilometers at the latitude of our cross section and the Bucak-Seydişehir cross section (McPhee et al., 2018; Figure 1c), for which there is no preserved field evidence. The structurally lowest thrust in our section is covered by Antalya-Alanya nappes, meaning that it is an unlikely structure to have accommodated tens of kilometers of shortening. We predict that such a floor thrust must crop out to the south of the exposed Geyikdağı rocks, but the location of that thrust remains unconstrained in the field. The Antalya-Alanya nappes are associated with Upper Cretaceous ophiolites that were emplaced onto the Taurides in Late Cretaceous to Paleocene time (Özgül, 1984). Those oceanic rocks are remnants of an ocean basin that once separated the African plate from the Taurides and demonstrate that the Geyikdağı nappe was bounded to the south by oceanic crust (Barrier & Vrielynck, 2008; Menant et al., 2016; Moix et al., 2008). This ocean basin subducted after the middle Eocene accretion of the Geyikdağı nappe to Anatolia and at the latitude of our Gündoğmuş-Hadim section, the sole thrust that accommodated the CW rotation likely developed into the oceanic subduction zone that consumed the eastern Mediterranean oceanic lithosphere.

Further to the north, at the latitude of the Bucak-Seydişehir section, the Beydağları platform forms the foreland of the Eocene belt. On that section line, we predict that the rotation was accommodated by around 45–60 km of shortening on thrust faults structurally below the Eocene fold-thrust belt. That must have resulted in thrusting of the Geyikdağı and higher nappes over the Beydağları platform rocks and part of the Antalya nappes. That shortening reshaped the Antalya nappes into narrow ~100 × 30 km long corridor that stretches northward from the city of Antalya to the city of Isparta (Figure 1).

The palinspastic reconstruction in this study requires a minor modification to the interpretation of the Bucak-Seydişehir section. There, McPhee et al. (2018) reconstructed Miocene, deeply rooted faults in the frontal part of the belt, between Beydağları and the Taurides. They had no solid constraint on structure at depth, and so in their structural model, they assumed the simplest interpretation in which exposed rocks at the surface were

underlain by their original stratigraphic underpinnings. Those were cross cut by Miocene thrust faults and displaced westward on a décollement. We suggest that instead of the original stratigraphic underpinnings, the frontal part of the belt is underpinned by underthrusted Beydağları platform rocks. With that modification, their cross section can viably accommodate the rotation. Miocene faulting may then have simply cross cut or reactivated the buried structures.

In summary, our combination of palinspastic reconstruction with cross-section balancing shows that the Taurides fold-thrust belt may contain upper crustal shortening that represent half or even a quarter of the convergence that was accommodated during nappe stacking. Without evidence from tectonic windows like the Menderes Massif, wholesale thrusting may go unnoticed if we rely on constraint from balanced cross sections based on fold-thrust belts alone. Our independent constraints suggest that in the Taurides wholesale underthrusting was the dominant process during subduction and accretion of the eastern part of Greater Adria and was interrupted by short-lived periods of perhaps only a few million years of accretion and rapid topographic growth during carbonate platform underthrusting. In mountain belts that contain far-traveled nappes, constraints on convergence based on plate circuits and paleomagnetic data are essential controls on the role of wholesale underthrusting. Balanced cross sections provide useful constraints on timing of accretion and modern orogenic architecture but may grossly underestimate convergence.

6. Conclusions

To assess the extent to which balanced cross sections provide a reliable estimate of accommodated convergence, we compared balanced cross sections across the Taurides fold-thrust belt in southern Turkey with a palinspastic, map-view reconstruction. To do this, we collected (i) paleomagnetic data to test previously published conclusions that the deepest nappe of the Taurides rotated ~40° CW, (ii) fault slip data to assess whether shortening in the belt was dip or oblique slip, and (iii) a new balanced cross section to assess along-strike cylindricity of structures. Our conclusions are summarized as follows:

1 Paleomagnetic and structural geological (fault slip) data, together with the balanced cross section point to a coherent nappe rotation of the Geyikdağı nappe in post-middle Eocene times, consistent with previous estimates. Our new paleomagnetic data define a $>$100 km long NW-SE trending rotated domain and show that the Taurides rotated as a coherent block, with no resolvable differential rotation within the Geyikdağı nappe fold-thrust belt.
2 Our balanced cross section across the Central Taurides documents at least 154 km of shortening, which includes a minimum of 27-km shortening on thrusts within the Geyikdağı nappe, a minimum of 70-km shortening on thrusts that emplaced the Aladağ and Bolkardağı nappes over the Geyikdağı nappe, and a minimum of 57-km shortening on thrust that emplaced the Bozkır nappes over the Aladağ and Bolkardağı nappe prior to 60 Ma. The thrusting in the Geyikdağı nappe has the same style and is equivalent to the documented structure of the northwestern part of the range. We find no evidence for Miocene thrusting in our study area, in contrast to the northwestern part of the range.
3 Fault zones within the Taurides fold-thrust belt record multiple phases of deformation but consistently contain evidence for a phase of westward and south-westward thrusting that has been highly oblique to Africa Eurasia convergence in Eocene to present times.
4 We reconstruct the CW rotation of the Taurides as a collision of the E-W trending Tauride block with a NW-SE trending trench during northward subduction. The most southeasterly part of the Geyikdağı must have entered the trench first, and that led to a norward-younging diachronous accretion of the Geyikdağı nappe to Anatolia, as the Taurides rotated about a pole in the southeast.
5 The rotation of the Geyikdağı nappe was accommodated between a floor and roof thrust. On the floor thrust, a southward-increasing amount of underthrusting (up to ~160 km) below the Taurides led to subduction of the Beydağları platform at the northwest end of the Tauride block and subduction of oceanic lithosphere at the southeast end of the Tauride block. The roof thrust accommodated northward increasing underthrusting (up to ~160 km) of the Geyikdağı nappe, below the far-traveled Aladağ, Bolkardağı, and Bozkır nappes.
6 Our map-view palinspastic reconstruction of the rotation predicts that as much as 200 km of convergence was likely taken up by wholesale underthrusting, for which there is very little record at the surface. Eocene accretion of crustal units accommodated a minimum 27 km in a few million years, yet built a significant nappe-stack.

7 Wholesale underthrusting was likely the dominant process in the accretion of the Tauride platforms and interpreted intervening basins to Anatolia and led to preservation of a highly incomplete accretionary record of convergence in the foreland fold-thrust belt. Reconstructions of convergence may use balanced cross sections as bare minimum estimates but are best combined with quantitative constraints from paleomagnetic data or plate circuits.

Data Statement

Data in this work are available as supplementary files. Supplementary file 01 contains a large scale version of our cross section and strip map (Figure 8a, main article) showing dip data we used to construct the section and a table of fault kinematic data. Supplementary file DS01 contains new paleomagnetic data and a compilation of published data as a file that can be used in the free Web-based tool paleomagnetism.org.

Acknowledgments
PJM and DJJvH acknowledge NWO Vidi grant 864.11.004 to DJJvH. We thank Nuretdin Kaymakcı for discussion. We thank reviewers Andrea Zanchi and Nicolas Espurt for constructive comments.

References

Aitchison, J. C., & Ali, J. R. (2012). India-Asia collision timing. *Proceedings of the National Academy of Sciences*, *109*(40), E2645–E2645. https://doi.org/10.1073/pnas.1207859109

Aldanmaz, E., Schmidt, M. W., Gourgaud, A., & Meisel, T. (2009). Mid-ocean ridge and supra-subduction geochemical signatures in spinel-peridotites from the Neotethyan ophiolites in SW Turkey: Implications for upper mantle melting processes. *Lithos*, *113*(3–4), 691–708. https://doi.org/10.1016/j.lithos.2009.03.010

Altiner, D., Özkan-Altiner, S., & Koçyiğit, A. (2000). Late Permian foraminiferal biofacies belts in Turkey: Palaeogeographic and tectonic implications. *Geological Society, London, Special Publications*, *173*(1), 83–96. https://doi.org/10.1144/GSL.SP.2000.173.01.04

Andrew, T., & Robertson, A. H. F. (2002). The Beysehir-Hoyran-Hadim nappes: Genesis and emplacement of Mesozoic marginal and oceanic units of their northern Neotethys in southern Turkey. *Journal of the Geological Society, London*, *159*(5), 529–543. https://doi.org/10.1144/0016-764901-157

Barnett-Moore, N., Font, E., & Neres, M. (2017). A reply to the comment on "Assessing discrepancies between previous plate kinematic models of Mesozoic Iberia and their constraints" by Barnett-Moore et al. *Tectonics*, *36*, 3286–3297. https://doi.org/10.1002/2017TC004760

Barnett-Moore, N., Hosseinpour, M., & Maus, S. (2016). Assessing discrepancies between previous plate kinematic models of Mesozoic Iberia and their constraints. *Tectonics*, *35*, 1843–1862. https://doi.org/10.1002/2015TC004019

Barrier, E., & Vrielynck, B. (2008). Atlas of paleotectonic maps of the Middle East (MEBE program). Commission for the Geological Map of the World.

Beaumont, C., Muñoz, J. A., Hamilton, J., & Fullsack, P. (2000). Factors controlling the alpine evolution of the central Pyrenees inferred from a comparison of observations and geodynamical models. *Journal of Geophysical Research*, *105*(B4), 8121–8145. https://doi.org/10.1029/1999JB900390

Berger, P., & Johnson, A. M. (1980). First-order analysis of deformation of a thrust sheet moving over a ramp. *Tectonophysics*, *70*(3–4), T9–T24. https://doi.org/10.1016/0040-1951(80)90276-0

Biryol, B. C., Beck, S. L., Zandt, G., & Özacar, a. A. (2011). Segmented African lithosphere beneath the Anatolian region inferred from teleseismic P-wave tomography. *Geophysical Journal International*, *184*(3), 1037–1057. https://doi.org/10.1111/j.1365-246X.2010.04910.x

Candan, O., Çetinkaplan, M., Oberhänsli, R., Rimmelé, G., & Akal, C. (2005). Alpine high-P/low-T metamorphism of the Afyon zone and implications for the metamorphic evolution of Western Anatolia, Turkey. *Lithos*, *84*(1–2), 102–124. https://doi.org/10.1016/j.lithos.2005.02.005

Çelik, Ö. F., Delaloye, M., & Feraud, G. (2006). Precise 40 Ar-39 Ar ages from the metamorphic sole rocks of the Tauride Belt ophiolites, southern Turkey: Implications for the rapid cooling history. *Geological Magazine*, *143*(02), 213. https://doi.org/10.1017/S0016756805001524

Çelik, Ö. F., & Delaloye, M. F. (2006). Characteristics of ophiolite-related metamorphic rocks in the Beysehir ophiolitic mélange (central Taurides, Turkey), deduced from whole rock and mineral chemistry. *Journal of Asian Earth Sciences*, *26*(5), 461–476. https://doi.org/10.1016/j.jseaes.2004.10.008

Cifelli, F., Mattei, M., & Rossetti, F. (2007). Tectonic evolution of arcuate mountain belts on top of a retreating subduction slab: The example of the Calabrian Arc. *Journal of Geophysical Research*, *112*, B09101. https://doi.org/10.1029/2006JB004848

Cinku, M. C., Hisarli, M., Yilmaz, Y., Ulker, B., Kaya, N., Oksum, E., et al. (2016). The tectonic history of the Nigde Kirsehir massif and the Taurides since the Late Mesozoic: Paleomagnetic evidence for two phase orogenic curvature in Central Anatolia. *Tectonics*, *35*, 772–811. https://doi.org/10.1002/2015TC003956

Cowgill, E., Forte, A. M., Niemi, N., Avdeev, B., Tye, A., Trexler, C., et al. (2016). Relict basin closure and crustal shortening budgets during continental collision: An example from Caucasus sediment provenance. *Tectonics*, *35*, 2918–2947. https://doi.org/10.1002/2016TC004295

Cowgill, E., Niemi, N. A., Forte, A. M., & Trexler, C. C. (2018). Reply to comment by Vincent et al. *Tectonics*, *37*, 1017–1028. https://doi.org/10.1002/2017TC004793

Davis, D., Suppe, J., & Dahlen, F. A. (1983). Mechanics of fold and thrust belts and accretionary wedges. *Journal of Geophysical Research*, *88*(B2), 1153–1172. https://doi.org/10.1029/JB088iB02p01153

DeCelles, P. G., Kapp, P., Gehrels, G. E., & Ding, L. (2014). Paleocene-Eocene foreland basin evolution in the Himalaya of southern Tibet and Nepal: Implications for the age of initial India-Asia collision. *Tectonics*, *33*, 824–849. https://doi.org/10.1002/2014TC003522

Deenen, M. H. L., Langereis, C. G., van Hinsbergen, D. J. J., & Biggin, A. J. (2011). Geomagnetic secular variation and the statistics of palaeomagnetic directions. *Geophysical Journal International*, *186*(2), 509–520. https://doi.org/10.1111/j.1365-246X.2011.05050.x

Delvaux, D., & Sperner, B. (2003). New aspects of tectonic stress inversion with reference to the TENSOR program. *Geological Society, London, Special Publications*, *212*(1), 75–100. https://doi.org/10.1144/GSL.SP.2003.212.01.06

DeMets, C., Iaffaldano, G., & Merkouriev, S. (2015). High-resolution Neogene and Quaternary estimates of Nubia-Eurasia-North America plate motion. *Geophysical Journal International*, *203*(1), 416–427. https://doi.org/10.1093/gji/ggv277

Demirtasli, E., Turhan, N., Bilgin, A. Z., & Selim, M. (1984). Geology of the Bolkar Mountains. Geology of the Taurus Belt. Proceedings of the International Symposium on the Geology of the Taurus Belt, Ankara, Turkey, 12–141.

Dilek, Y., Furnes, H., & Shallo, M. (2007). Suprasubduction zone ophiolite formation along the periphery of Mesozoic Gondwana. *Gondwana Research*, *11*(4), 453–475. https://doi.org/10.1016/j.gr.2007.01.005

Fisher, R. (1953). Dispersion on a Sphere. *Proceedings of the Royal Society A: Mathematical, Physical and Engineering Sciences*, *217*(1130), 295–305. https://doi.org/10.1098/rspa.1953.0064

Gaina, C., Torsvik, T. H., van Hinsbergen, D. J. J., Medvedev, S., Werner, S. C., & Labails, C. (2013). The African plate: A history of oceanic crust accretion and subduction since the Jurassic. *Tectonophysics*, *604*, 4–25. https://doi.org/10.1016/j.tecto.2013.05.037

Gansser, A. (1980). The significance of the Himalayan suture zone. *Tectonophysics*, *62*(1–2), 37–52. https://doi.org/10.1016/0040-1951(80)90134-1

Gessner, K., Ring, U., Passchier, C. W., & Gungor, T. (2001). How to resist subduction: Evidence for large-scale out-of-sequence thrusting during Eocene collision in western Turkey. *Journal of the Geological Society*, *158*(5), 769–784. https://doi.org/10.1144/jgs.158.5.769

Gürer, D., Plunder, A., Kirst, F., Corfu, F., Schmid, S. M., & van Hinsbergen, D. J. J. (2018). A long-lived Late Cretaceous-early Eocene extensional province in Anatolia? Structural evidence from the Ivriz detachment, southern central Turkey. *Earth and Planetary Science Letters*, *481*, 111–124. https://doi.org/10.1016/j.epsl.2017.10.008

Gürer, D., & van Hinsbergen, D. J. J. (2018). Diachronous demise of the Neotethys Ocean as a driver for non-cylindrical orogenesis in Anatolia. *Tectonophysics*. https://doi.org/10.1016/j.tecto.2018.06.005

Gürer, D., van Hinsbergen, D. J. J., Matenco, L., Corfu, F., & Cascella, A. (2016). Kinematics of a former oceanic plate of the Neotethys revealed by deformation in the Ulukışla basin (Turkey). *Tectonics*, *35*, 2385–2416. https://doi.org/10.1002/2016TC004206

Gürer, D., van Hinsbergen, D. J. J., Özkaptan, M., Creton, I., Koymans, M. R., Cascella, A., et al. (2018). Paleomagnetic constraints on the timing and distribution of Cenozoic rotations in central and eastern Anatolia. *Solid Earth*, *9*(2), 295–322. https://doi.org/10.5194/se-9-295-2018

Gutnic, M., Monod, O., Poisson, A., & Dumont, J.-F. (1979). Géologie des Taurides Occidentales (Turquie). *Mémoires de La Société Géologique de France*, *137*, 1–112.

Huang, W., Van Hinsbergen, D. J. J., Lippert, P. C., Guo, Z., & Dupont-Nivet, G. (2015). Paleomagnetic tests of tectonic reconstructions of the India-Asia collision zone. *Geophysical Research Letters*, *42*, 2642–2649. https://doi.org/10.1002/2015GL063749

Ingalls, M., Rowley, D. B., Currie, B., & Colman, A. S. (2016). Large-scale subduction of continental crust implied by India-Asia mass-balance calculation. *Nature Geoscience*, *9*(11), 848–853. https://doi.org/10.1038/ngeo2806

Johnson, C. L., Constable, C. G., Tauxe, L., Barendregt, R., Brown, L. L., Coe, R. S., et al. (2008). Recent investigations of the 0–5 Ma geomagnetic field recorded by lava flows. *Geochemistry, Geophysics, Geosystems*, *9*, Q04032. https://doi.org/10.1029/2007GC001696

Kalyoncuoğlu, Ü. Y., Elitok, Ö., Dolmaz, M. N., & Anadolu, N. C. (2011). Geophysical and geological imprints of southern Neotethyan subduction between Cyprus and the Isparta angle, SW Turkey. *Journal of Geodynamics*, *52*(1), 70–82. https://doi.org/10.1016/j.jog.2010.12.001

Kirschvink, J. L. (1980). The least-squares line and plane and the analysis of palaeomagnetic data. *Geophysical Journal International*, *62*(3), 699–718. https://doi.org/10.1111/j.1365-246X.1980.tb02601.x

Kissel, C., Averbuch, O., de Lamotte, D. F., Monod, O., & Allerton, S. (1993). First paleomagnetic evidence for a post-Eocene clockwise rotation of the Western Taurides thrust belt east of the Isparta reentrant (southwestern Turkey). *Earth and Planetary Science Letters*, *117*(1-2), 1–2), 1–14. https://doi.org/10.1016/0012-821X(93)90113-N

Koç, A., Kaymakci, N., Van Hinsbergen, D. J. J., & Kuiper, K. F. (2017). Miocene tectonic history of the central Tauride intramontane basins, and the paleogeographic evolution of the Central Anatolian Plateau. *Global and Planetary Change*, *158*, 83–102. https://doi.org/10.1016/j.gloplacha.2017.09.001

Koç, A., Kaymakci, N., van Hinsbergen, D. J. J., Kuiper, K. F., & Vissers, R. L. M. (2012). Tectono-Sedimentary evolution and geochronology of the middle Miocene Altınapa Basin, and implications for the late Cenozoic uplift history of the Taurides, southern Turkey. *Tectonophysics*, *532-535*, 134–155. https://doi.org/10.1016/j.tecto.2012.01.028

Koç, A., Kaymakci, N., van Hinsbergen, D. J. J., & Vissers, R. L. M. (2016). A Miocene onset of the modern extensional regime in the Isparta angle: Constraints from the Yalvaç Basin (southwest Turkey). *International Journal of Earth Sciences*, *105*(1), 369–398. https://doi.org/10.1007/s00531-014-1100-z

Koç, A., van Hinsbergen, D. J. J., Kaymakci, N., & Langereis, C. G. (2016). Late Neogene oroclinal bending in the central Taurides: A record of terminal eastward subduction in southern Turkey? *Earth and Planetary Science Letters*, *434*(1), 75–90. https://doi.org/10.1016/j.epsl.2015.11.020

Koç, A., van Hinsbergen, D. J. J., & Langereis, C. G. (2018). Rotations of normal fault blocks quantify extension in the Central Tauride intramontane basins, SW Turkey. *Tectonics*, *37*, 2307–2327. https://doi.org/10.1029/2018TC005112

Koymans, M. R., Langereis, C. G., Pastor-Galán, D., & van Hinsbergen, D. J. J. (2016). Paleomagnetism.org: An online multi-platform open source environment for paleomagnetic data analysis. *Computers and Geosciences*, *93*, 127–137. https://doi.org/10.1016/j.cageo.2016.05.007

Lefebvre, C., Meijers, M. J. M., Kaymakci, N., Peynircioğlu, A., Langereis, C. G., & van Hinsbergen, D. J. J. (2013). Reconstructing the geometry of central Anatolia during the late Cretaceous: Large-scale Cenozoic rotations and deformation between the Pontides and Taurides. *Earth and Planetary Science Letters*, *366*, 83–98. https://doi.org/10.1016/j.epsl.2013.01.003

Li, S., Advokaat, E. L., van Hinsbergen, D. J. J., Koymans, M., Deng, C., & Zhu, R. (2017). Paleomagnetic constraints on the Mesozoic-Cenozoic paleolatitudinal and rotational history of Indochina and South China: Review and updated kinematic reconstruction. *Earth-Science Reviews*, *171*, 58–77. https://doi.org/10.1016/j.earscirev.2017.05.007

Long, S., McQuarrie, N., Tobgay, T., & Grujic, D. (2011). Geometry and crustal shortening of the Himalayan fold-thrust belt, eastern and central Bhutan. *Geological Society of America Bulletin*, *123*(7–8), 1427–1447. https://doi.org/10.1130/B30203.1

Mackintosh, P. W., & Robertson, A. H. F. (2013). Sedimentary and structural evidence for two-phase Upper Cretaceous and Eocene emplacement of the Tauride thrust sheets in central southern Turkey. *Geological Society, London, Special Publications*, *372*(1), 299–322. https://doi.org/10.1144/SP372.2

Maffione, M., & van Hinsbergen, D. J. J. (2018). Reconstructing plate boundaries in the Jurassic neo-Tethys from the east and west Vardar ophiolites (Greece and Serbia). *Tectonics*, *37*, 858–887. https://doi.org/10.1002/2017TC004790

Maffione, M., van Hinsbergen, D. J. J., de Gelder, G. I. N. O., van der Goes, F. C., & Morris, A. (2017). Kinematics of Late Cretaceous subduction initiation in the neo-Tethys Ocean reconstructed from ophiolites of Turkey, Cyprus, and Syria. *Journal of Geophysical Research: Solid Earth*, *122*, 3953–3976. https://doi.org/10.1002/2016JB013821

McFadden, P. L., & McElhinny, M. W. (1988). The combined analysis of remagnetization circles and direct observations in palaeomagnetism. *Earth and Planetary Science Letters*, *87*(1–2), 161–172. https://doi.org/10.1016/0012-821X(88)90072-6

McFadden, P. L., & McElhinny, M. W. (1990). Classification of the reversal test in palaeomagnetism. *Geophysical Journal International*, *103*(3), 725–729. https://doi.org/10.1111/j.1365-246X.1990.tb05683.x

McPhee, P. J., Altıner, D., & van Hinsbergen, D. J. J. (2018). First balanced cross section across the Taurides fold-thrust belt: Geological constraints on the subduction history of the Antalya slab in Southern Anatolia. *Tectonics*, *37*. https://doi.org/10.1029/2017TC004893

McPhee, P. J. (2018). Preparing the ground for plateau growth: Central Anatolian uplift in the context of Tauride and Cypriot orogenesis, Utrecht Studies in Earth Sciences 161 (196 pp.).

McQuarrie, N. (2002). The kinematic history of the central Andean fold-thrust belt, Bolivia: Implications for building a high plateau. *Bulletin of the Geological Society of America*, *114*(8), 950–963. https://doi.org/10.1130/0016-7606(2002)114<0950:TKHOTC>2.0.CO;2

McQuarrie, N., & van Hinsbergen, D. J. J. (2013). Retrodeforming the Arabia-Eurasia collision zone: Age of collision versus magnitude of continental subduction. *Geology*, *41*(3), 315–318. https://doi.org/10.1130/G33591.1

Meijers, M. J. M., van Hinsbergen, D. J. J., Dekkers, M. J., Altıner, D., Kaymakcı, N., & Langereis, C. G. (2011). Pervasive Palaeogene remagnetization of the central Taurides fold-and-thrust belt (southern Turkey) and implications for rotations in the Isparta angle. *Geophysical Journal International*, *184*(3), 1090–1112. https://doi.org/10.1111/j.1365-246X.2010.04919.x

Menant, A., Jolivet, L., & Vrielynck, B. (2016). Kinematic reconstructions and magmatic evolution illuminating crustal and mantle dynamics of the eastern Mediterranean region since the Late Cretaceous. *Tectonophysics*, *675*, 103–140. https://doi.org/10.1016/j.tecto.2016.03.007

Moix, P., Beccaletto, L., Kozur, H. W., Hochard, C., Rosselet, F., & Stampfli, G. M. (2008). A new classification of the Turkish terranes and sutures and its implication for the paleotectonic history of the region. *Tectonophysics*, *451*(1–4), 7–39. https://doi.org/10.1016/j.tecto.2007.11.044

Monod, O. (1977). Recherches geologique dans les Taurus occidental au sud de Beysehir (Turquie). PhD thesis. Universite de Paris-Sud, Orsay.

Muñoz, J. A. (1992). Evolution of a continental collision belt: ECORS-Pyrenees crustal balanced cross-section. In K. R. McClay (Ed.), *Thrust tectonics*, (pp. 235–246). Dordrecht: Springer Netherlands. https://doi.org/10.1007/978-94-011-3066-0_21

Nicol, A., & Beavan, J. (2003). Shortening of an overriding plate and its implications for slip on a subduction thrust, central Hikurangi Margin, New Zealand. *Tectonics*, *22*(6), 1070. https://doi.org/10.1029/2003TC001521

Okay, A. I. (1984). Distribution and characteristics of the north-west Turkish blueschists. *Geological Society, London, Special Publications*, *17*(1), 455–466. https://doi.org/10.1144/GSL.SP.1984.017.01.33

Okay, A. I. (1986). High-pressure/low-temperature metamorphic rocks of Turkey. *Geological Society of America Memoirs*, *164*, 333–347. https://doi.org/10.1130/MEM164-p333

Oncken, O., Hindle, D., Kley, J., Elger, K., Victor, P., & Schemmann, K. (2006). Deformation of the Central Andean Upper Plate System—Facts, fiction, and constraints for plateau models. In O. Oncken, G. Franz, P. Giese, H. Götze, V. Ramos, M. Strecker, & P. Wigger (Eds.), *The Andes, active subduction orogeny* (pp. 3–27). Berlin, Heidelberg: Springer. https://doi.org/10.1007/978-3-540-48684-8_1

Özdamar, Ş., Billor, M. Z., Sunal, G., Esenli, F., & Roden, M. F. (2013). First U-Pb SHRIMP zircon and 40Ar/39Ar ages of metarhyolites from the Afyon-Bolkardag Zone, SW Turkey: Implications for the rifting and closure of the Neo-Tethys. *Gondwana Research*, *24*(1), 377–391. https://doi.org/10.1016/j.gr.2012.10.006

Özer, S., & Sözbilir, H. (2003). Presence and tectonic significance of Cretaceous rudist species in the so-called Permo-Carboniferous Goktepe formation, Central Menderes metamorphic massif, western Turkey. *International Journal of Earth Sciences*, *92*(3), 397–404. https://doi.org/10.1007/s00531-003-0333-z

Özgül, N. (1976). Some geological aspects of the Taurus orogenic belt (Turkey). *Bulletin of the Geological Society of Turkey*, 65–78.

Özgül, N. (1984). Stratigraphy and tectonic evolution of the central Taurus. In *Proceedings of International Symposium on the Geology of the Taurus Belt, 1983* (pp. 77–90). General Directorate of Mineral Research and Exploration (MTA).

Parlak, O., Karaoğlan, F., Rızaoğlu, T., Klötzli, U., Koller, F., & Billor, Z. (2013). U-Pb and 40Ar-39Ar geochronology of the ophiolites and granitoids from the Tauride belt: Implications for the evolution of the inner Tauride suture. *Journal of Geodynamics*, *65*, 22–37. https://doi.org/10.1016/j.jog.2012.06.012

Piper, J. D. A., Gürsoy, H., Tatar, O., İşseven, T., & Koçyiğit, A. (2002). Palaeomagnetic evidence for the Gondwanian origin of the Taurides and rotation of the Isparta angle, southern Turkey. *Geological Journal*, *37*(4), 317–336. https://doi.org/10.1002/gj.920

Plunder, A., Agard, P., Chopin, C., Pourteau, A., & Okay, A. I. (2015). Accretion, underplating and exhumation along a subduction interface: From subduction initiation to continental subduction (Tavşanlı zone, W. Turkey). *Lithos*, *226*, 233–254. https://doi.org/10.1016/j.lithos.2015.01.007

Pourteau, A., Candan, O., & Oberhänsli, R. (2010). High-pressure metasediments in Central Turkey: Constraints on the Neotethyan closure history. *Tectonics*, *29*, TC5004. https://doi.org/10.1029/2009TC002650

Pourteau, A., Scherer, E. E., Schorn, S., Bast, R., Schmidt, A., & Ebert, L. (2018). Thermal evolution of an ancient subduction interface revealed by Lu-Hf garnet geochronology, Halilbağı Complex (Anatolia). *Geoscience Frontiers*. https://doi.org/10.1016/j.gsf.2018.03.004

Pourteau, A., Sudo, M., Candan, O., Lanari, P., Vidal, O., & Oberhänsli, R. (2013). Neotethys closure history of Anatolia: Insights from 40Ar-39Ar geochronology and P-T estimation in high-pressure metasedimentary rocks. *Journal of Metamorphic Geology*, *31*(6), 585–606. https://doi.org/10.1111/jmg.12034

Ring, U., Will, T., Glodny, J., Kumerics, C., Gessner, K., Thomson, S., et al. (2007). Early exhumation of high-pressure rocks in extrusion wedges: Cycladic blueschist unit in the eastern Aegean, Greece, and Turkey. *Tectonics*, *26*, TC2001. https://doi.org/10.1029/2005TC001872

Robertson, A. H. F. (2004). Development of concepts concerning the genesis and emplacement of Tethyan ophiolites in the Eastern Mediterranean and Oman regions. *Earth-Science Reviews*, *66*(3–4), 331–387. https://doi.org/10.1016/j.earscirev.2004.01.005

Robertson, A. H. F., Parlak, O., & Ustaömer, T. (2009). Melange genesis and ophiolite emplacement related to subduction of the northern margin of the Tauride-Anatolide continent, central and western Turkey. *Geological Society, London, Special Publications*, *311*(1), 9–66. https://doi.org/10.1144/sp311.2

Roeder, D. (2010). Fold-thrust belts at peak oil. *Geological Society, London, Special Publications*, *348*(107), 7–31. https://doi.org/10.1144/SP348.2

Rowley, D., & Ingalls, M. (2017). Reply to "Unfeasible subduction?". *Nature Geoscience*, *10*(12), 879–880. https://doi.org/10.1038/s41561-017-0016-1

Schepers, G., Spakman, W., Kosters, M. E., Boschman, L. M., McQuarrie, N., & van Hinsbergen, D. J. J. (2017). South-American plate advance and forced Andean trench retreat as drivers for transient flat subduction episodes. *Nature Communications*, *8*, 1–9. https://doi.org/10.1038/ncomms15249.

Sengör, A. M., & Yilmaz, Y. (1981). Tethyan evolution of Turkey: A plate tectonic approach. *Tectonophysics*, *75*(3–4), 181–241. https://doi.org/10.1016/0040-1951(81)90275-4

Seton, M., Müller, R. D., Zahirovic, S., Gaina, C., Torsvik, T., Shephard, G., et al. (2012). Global continental and ocean basin reconstructions since 200Ma. *Earth-Science Reviews*, *113*(3–4), 212–270. https://doi.org/10.1016/j.earscirev.2012.03.002

Seyitoglu, G., Icsik, V., Gürbüz, E., & Gürbüz, A. (2017). The discovery of a low-angle normal fault in the Taurus Mountains: The İvriz detachment and implications concerning the Cenozoic geology of southern Turkey. *Turkish Journal of Earth Sciences*, *26*, 189–205. https://doi.org/10.3906/yer-1610-11

Stampfli, G., Marcoux, J., & Baud, A. (1991). Tethyan margins in space and time. *Palaeogeography, Palaeoclimatology, Palaeoecology*, *87*(1–4), 373–409. https://doi.org/10.1016/0031-0182(91)90142-E

Suppe, J. (1983). Geometry and kinematics of fault-bend folding. *American Journal of Science*, *283*(7), 684–721. https://doi.org/10.2475/ajs.283.7.684

Takin, M. (1972). Iranian geology and continental drift in the Middle East. *Nature*, *235*(5334), 147–150. https://doi.org/10.1038/235147a0

Tate, G. W., McQuarrie, N., van Hinsbergen, D. J. J., Bakker, R. R., Harris, R., & Jiang, H. (2015). Australia going down under: Quantifying continental subduction during arc-continent accretion in Timor-Leste. *Geosphere*, *11*(6), 1860–1883. https://doi.org/10.1130/GES01144.1

Tauxe, L. (2010). *Essentials of Paleomagnetism*. Oakland, CA: University of California Press.

Tauxe, L., & Watson, G. S. (1994). The fold test: An eigen analysis approach. *Earth and Planetary Science Letters*, *122*(3–4), 331–341. https://doi.org/10.1016/0012-821X(94)90006-X

Topuz, G., Celik, O. F., Sengör, A. M., Altintas, I. E., Zack, T., Rolland, Y., et al. (2013). Jurassic ophiolite formation and emplacement as backstop to a subduction-accretion complex in Northeast Turkey, the Refahiye ophiolite, and relation to the Balkan ophiolites. *American Journal of Science*, *313*(10), 1054–1087. https://doi.org/10.2475/10.2013.04

Torsvik, T. H., Van der Voo, R., Preeden, U., Mac Niocaill, C., Steinberger, B., Doubrovine, P. V., et al. (2012). Phanerozoic polar wander, palaeogeography and dynamics. *Earth-Science Reviews*, *114*(3–4), 325–368. https://doi.org/10.1016/j.earscirev.2012.06.007

van der Meer, D. G., van Hinsbergen, D. J. J., & Spakman, W. (2018). Atlas of the underworld: Slab remnants in the mantle, their sinking history, and a new outlook on lower mantle viscosity. *Tectonophysics*, *723*(2011), 309–448. https://doi.org/10.1016/j.tecto.2017.10.004

van Hinsbergen, D. J. J., Hafkenscheid, E., Spakman, W., Meulenkamp, J. E., & Wortel, R. (2005). Nappe stacking resulting from subduction of oceanic and continental lithosphere below Greece. *Geology*, *33*(4), 325. https://doi.org/10.1130/G20878.1

van Hinsbergen, D. J. J., Kaymakci, N., Spakman, W., & Torsvik, T. H. (2010). Reconciling the geological history of western Turkey with plate circuits and mantle tomography. *Earth and Planetary Science Letters*, *297*(3–4), 674–686. https://doi.org/10.1016/j.epsl.2010.07.024

van Hinsbergen, D. J. J., Lippert, P. C., Dupont-Nivet, G., McQuarrie, N., Doubrovine, P. V., Spakman, W., et al. (2012a). Greater India Basin hypothesis and a two-stage Cenozoic collision between India and Asia. *Proceedings of the National Academy of Sciences*, *109*(20), 7659–7664. https://doi.org/10.1073/pnas.1117262109

van Hinsbergen, D. J. J., Lippert, P. C., Dupont-Nivet, G., McQuarrie, N., Doubrovine, P. V., Spakman, W., et al. (2012b). Reply to Aitchison and Ali: Reconciling Himalayan ophiolite and Asian magmatic arc records with a two-stage India-Asia collision model. *Proceedings of the National Academy of Sciences*, *109*(40), E2646–E2646. https://doi.org/10.1073/pnas.1208836109

van Hinsbergen, D. J. J., Lippert, P. C., & Huang, W. (2017). Unfeasible subduction? *Nature Geoscience*, *10*(12), 878–879. https://doi.org/10.1038/s41561-017-0017-0

van Hinsbergen, D. J. J., Lippert, P. C., Li, S., Huang, W., Advokaat, E. L., & Spakman, W. (2018). Reconstructing Greater India: Paleogeographic, kinematic, and geodynamic perspectives. *Tectonophysics*. https://doi.org/10.1016/j.tecto.2018.04.006

van Hinsbergen, D. J. J., Maffione, M., Plunder, A., Kaymakcı, N., Ganerød, M., Hendriks, B. W. H., et al. (2016). Tectonic evolution and paleogeography of the Kırşehir block and the Central Anatolian Ophiolites, Turkey. *Tectonics*, *35*, 983–1014. https://doi.org/10.1002/2015TC004018

van Hinsbergen, D. J. J., & Schmid, S. M. (2012). Map view restoration of Aegean-west Anatolian accretion and extension since the Eocene. *Tectonics*, *31*, TC5005. https://doi.org/10.1029/2012TC003132

van Hinsbergen, D. J. J., Spakman, W., Vissers, R. L. M., & van der Meer, D. G. (2017). Comment on "assessing discrepancies between previous plate kinematic models of Mesozoic Iberia and their constraints" by Barnett-Moore et Al. *Tectonics*, *36*, 3277–3285. https://doi.org/10.1002/2016TC004418

Vincent, S. J., Saintot, A., Mosar, J., Okay, A. I., & Nikishin, A. M. (2018). Comment on "Relict Basin closure and crustal shortening budgets during continental collision: An example from Caucasus sediment provenance" by Cowgill et al. (2016). *Tectonics*, *37*, 1006–1016. https://doi.org/10.1002/2017TC004515

Vissers, R. L. M., van Hinsbergen, D. J. J., van der Meer, D. G., & Spakman, W. (2016). Cretaceous slab break-off in the Pyrenees: Iberian plate kinematics in paleomagnetic and mantle reference frames. *Gondwana Research*, *34*, 49–59. https://doi.org/10.1016/j.gr.2016.03.006

Whitney, D. L., Teyssier, C., Fayon, A. K., Hamilton, M. A., & Heizler, M. (2003). Tectonic controls on metamorphism, partial melting, and intrusion: Timing and duration of regional metamorphism and magmatism in the Nigde massif, Turkey. *Tectonophysics*, *376*(1–2), 36–60.

Whitney, D. L., Teyssier, C., Seaton, N. C. A., & Fornash, K. F. (2014). Petrofabrics of high-pressure rocks exhumed at the slab-mantle interface from the "point of no return" in a subduction zone (Sivrihisar, Turkey). *Tectonics*, *33*, 2315–2341. https://doi.org/10.1002/2014TC003677

Woodward, N. B., Boyer, S. E., & Suppe, J. (1989). *Balanced geological cross-sections: An essential technique in geological research and exploration*, *International Geological Congress, Short Course in Geology* (Vol. 6). Washington, DC: American Geophysical Union. https://doi.org/10.1029/SC006

Zijderveld, J. D. A. (1967). A. C. demagnetization of rocks: Analysis of results. In D. W. Collinson, K. M. Creer, & S. K. Runcorn (Eds.), *Methods in palaeomagnetism* (pp. 254–286). Amsterdam, Netherlands: Elsevier. https://doi.org/10.1016/B978-1-4832-2894-5.50049-5